LAPPEENRANTA UNIVERSITY OF TECHNOLOGY

LUT School of Engineering Science

Master's Double Degree Program in Chemical Engineering

Anton Poll

MASS TRANSFER AND REACTION KINETICS IN SINGLE DROPLET SYSTEMS

Examiners: Professor Tuomas Koiranen

Lic.Sc. (Tech.) Esko Lahdenpera

Abstract

Anton Poll
Mass transfer and reaction kinetics in single droplet systems
School of Engineering Science
Master's Double Degree Program in Chemical Engineering
2016
Lappeenranta University of Technology
Tables: 5, figures: 23, appendices: 3
Examiners: professor Tuomas Koiranes, Lis.Sc. (Tech.) Esko Lahdenpera
Keywords: mass, transfer, kinetics, droplet, solvent, extraction, complex, organic, aqueous, resistance.

As reactive extraction grown more and more popular in a variety of technological applications, optimizing its performance becomes more and more important. The process of complex formation is affected by a great number of both physical and chemical properties of all the components involved, and sometimes their interference with one another makes improving the effectiveness of such processes very difficult. In this Master's Theses, the processes of complex formation between the aqueous phase - represented by copper sulfate water solution, and organic phase – represented by Acorga M5640 solvent extractor, were studied in order to establish the effect these components have on reactive extraction performance and to determine which step is bottlenecking the process the most.

List of symbols and abbreviations

A	droplet surface area, m^3
c	concentration, kg/m^3
c^*	dimensionless mean concentration, –
C_D	drag coefficient, –
d_P	drop diameter, m
D	molecular diffusivity, m^2/s
D^*	ratio of diffusivities $D_{A,d}/D_{A,c}$, –
f	correction factor, -
F	force, N
g	gravitational acceleration, m/s^2
k_B	Boltzmann constant, $1.38 \cdot 10^{-23}$, J/K
k_o	overall mass transfer coefficient, m/s
k_c	mass transfer coefficient in the continuous phase, m/s
k_d	mass transfer coefficient in the dispersed phase, m/s
K^*	partition coefficient, –
$\dot{m}$	mass flux, $kg/(m^2\ s)$
M	mass of the drop, kg
R	droplet radius, m
t	time, s
T	temperature, K
v	velocity, m/s
V	drop volume, m^3
α	diffusivity factor, –
β	mass transfer coefficient, m/s
δ	boundary layer thickness, m
Δ_c	fractional resistance in the continuous phase, %
Δ_d	fractional resistance in the dispersed phase, %
Δ_r	fractional resistance due to the reaction, %
κ	virtual mass coefficient, –
μ	dynamic viscosity, $Pa \cdot s$
μ^*	viscosity ratio μ_d/μ_c, –

ρ	density, kg/m^3
ρ^*	density ratio ρ_d/ρ_c, –
$\Delta\rho$	density difference $\lvert\rho_d - \rho_c\rvert$; kg/m^3
γ	interfacial tension, N/m
χ	volume fraction
A	transfer component
B	buoyancy
c	continuous phase
cr	critical
d	dispersed phase, droplet
f	formation
G	gravitation
i	inertia
I	interface
o	overall
org	organic
P	particle, droplet
ra	reacceleration
s	solute
t	terminal
wat	water
Fo	Fourier number $Fo = D_s t/R^2$
Mo	Morton number $Mo = g\mu_c^2\Delta\rho/(\rho_c^2\gamma^3)$
Pe	Peclet number $Pe = v_t d_p/D_s$
Re	Reynolds number $Re = v_t d_p \rho_c/\mu_c$
Sc	Schmidt number $Sc = \mu_c/(\rho_c D_{s,c})$
Sh	Sherwood number $Sh = \beta d_p/D_s$
We	Weber number $We = v_t^2 d_p \rho_c/\gamma$

Table of contents

1. Introduction……...6
2. General applications of reactive extraction……7
3. Reactive extraction……8
   3.1 Complex formation……10
   3.2 Reaction equations and reaction kinetics……11
   3.3 Reaction mechanisms for Acorga……...12
4. Single droplets in liquid-liquid systems……...15
   4.1 Fluid dynamics……...15
      4.1.1 General description……15
      4.1.2 Regimes of flow……16
      4.1.3 Terminal velocity……...18
   4.2 Mass transfer……..18
      4.2.1 General description……18
      4.2.2 External/internal problems……20
      4.2.3 Marangoni convections and internal circulations……23
   4.3 Additional factors……..……26
5. Single droplets experimental setup……..…..27
   5.1 Different setups……...27
   5.2 Droplet formation, settling and coalescence……..…30
6. Experimental part……..……32
   6.1 Experimental setup……32
   6.2 Analytics……...…..35
   6.3 Experimental plan……...…37
7. Results and discussions……41
8. Conclusion……50

References……..……51

Appendices

Appendix I

Appendix II

Appendix III

1 Introduction

As old as reactive extraction may be, the process of improving the efficiency of the process has never stopped. Nowadays, after centuries of evolution, reactive extraction is used in a great number of fields, but the search for better performance continues. The processes affecting the efficiency of reactive extraction are of different natures: some come from the physical properties of the involved components, others are determined by the chemistry. Still, these processes don't just influence the extraction directly – they often interfere with one another, strengthening each other's effects or, on the contrary, minimizing them. The complexity of physics and chemistry involved sometimes doesn't let scientists investigate them easily. In order to find some extra performance, they try to determine the components and processes that create the most resistance to the process, slowing the reaction down and decreasing the efficiency. This task is extremely important – while some improvements may seem simpler than others, they may not cause the desired gain in performance, because the effect on the overall process is minimal.

In this Thesis, copper extraction by Acorga M5640 was researched and the fractional resistances of both components were determined. A number of parameters, such as concentrations, feedrates etc. were varied to gain better coverage of the problem. As a result, it was determined, that for normal phase processes, when the organic solution is dispersed, the mass transfer rate values increase with feedrate, bigger needle diameters and greater copper sulfate concentrations, while being indifferent to the column height. For inverted phase experiments, neither the needle diameters nor the copper sulfate concentrations are effecting the mass transfer rate. The resistance proved to be due to the reaction itself rather than lying in the dispersed or the continuous phase, and while the fractional resistances in the phases are noticeable in the experiments with high copper sulfate concentrations in normal phase mode. In case of low copper sulfate concentrations or the inversion of the phases, the fractional resistances in both the dispersed and the continuous phases become almost non-existent. Also, a correlation between the droplet diameter and the Sherwood number was estimated with a fit of 0.92.

2 Applications of reactive extraction

The history of extraction processes spans for centuries. Scientists report about extraction instructions that were documented by Sumerian texts dated 2100 BC, and some extraction pots found near Baghdad were estimated 3500 BC of age [1]. These primitive vessels were designed to contain mixtures of different chemicals and utilize the difference in boiling temperatures to evaporate the required component and condensate it afterwards. Though being the first step of extraction processes, they had to go through several thousand years of evolution until the Middle Ages, where different organic solvents like ethanol, acids and amalgams were used to extract and purify different metals, thus becoming the first examples of chemical extraction and separation. For a long time, reactive solvent extraction was used for extraction of uranium as well as of pyrometallurgically difficult-to-separate metals, such as niobium, tantalum, zirconium and others [2].

However, the industrial breakthrough that helped to spread reactive solvent extraction widely happened later, in 1960s, when liquid ion exchanger chemicals were introduced to perform the separation of copper from iron, allowing copper recovery from low-grade ores. Since then, reactive extraction have already been used in a great variety of applications, such as pharmaceutical industries (penicillin, vitamins, organic acids, etc.), petrochemical (caprolactam) and biochemical fields, as well as hydrometallurgy and environmental chemistry (heavy metals, inorganic acids) [3].

3 Reactive extraction

Reactive solvent systems are determined by the organic phase consisting of the liquid ion exchanger mixed with the organic diluent. In contrast to single solvent systems, where a bulk organic chemical is used to extract the solute, reactive solvent systems require adjustments in physical properties, such as density, viscosity and others. To achieve those, nonaromatic organic diluents that are immiscible in water are used. By mixing them with the ion exchangers, that are usually very dense or even solid, a low-density and low-viscosity solution is created, which allows the dispersed phase to travel through it. Choosing the correct reactive solvent is critical to the performance of the whole system. According to Bart and Stevens [2], there is a great number of characteristics that should be taken into consideration, such as:

- *Selectivity* – one of the most important qualities of the solvent. By increasing the selectivity, the general time required to achieve the extraction can be reduced, as well the number of stages of the process can be minimized;
- *Capacity* – yet another critical parameter, as greater capacity results in lower solvent-to-feed ratios. Capacity should be balanced with the selectivity properly by adjusting the temperature of the process, since higher temperatures can increase the capacity of the solvent but reduce its selectivity and vice versa;
- *Recoverability.* It is desirable that the recoverability of the solvent could be as simple as possible, preferably by distillation or a combination of distillation and stripping;
- *Density.* Higher density differences between the phases simplify the settling of the phases, while processes with lower differences may require additional means of extraction, such as centrifugal extractors;
- *Viscosity.* Low viscosities make the solutions easier to pump as well as improve the settling of the phases;
- *Solubility.* If the non-solute and solvent have high mutual solubility, additional separation measures can be required;
- *Interfacial tension.* Yet another parameter that should be balanced properly – while high interfacial tension can improve coalescence, resulting in high capacities, low interfacial tension helps to increase the interfacial area (while, however, requiring additional phase separation);

- *Toxicity, flammability and corrosivity.* These parameters effect the general safety of the process for workers, the impact of the process on the environment, as well as the lifespan of the equipment that is used.

The equipment used in reactive extraction can be divided into two main groups: non-agitated columns and agitated extractors. The simplest design is a non-agitated spray column (see Figure 1). While being cheap to design and manufacture, it has a very low efficiency due to large-scale axial mixing. In order to improve the performance, different designs of internals were created to increase the mass transfer by facilitating breakage and coalescence of the dispersed phase. However, in non-agitated columns the performance is heavily determined by the flowrates of the phases and their physical properties, such as density and viscosity. To achieve better flexibility of the process, agitated extractors were introduced. The mass transfer efficiency is improved by increasing the dispersed phase breakage and coalescence via mechanical means. Though being more complex in design, installation and maintenance, agitated extractors can help to control various parameters, e.g. droplet size, independently from the feedrates of the phases, thus improving the performance. Various designs of agitated extractors are represented on Figure 2.

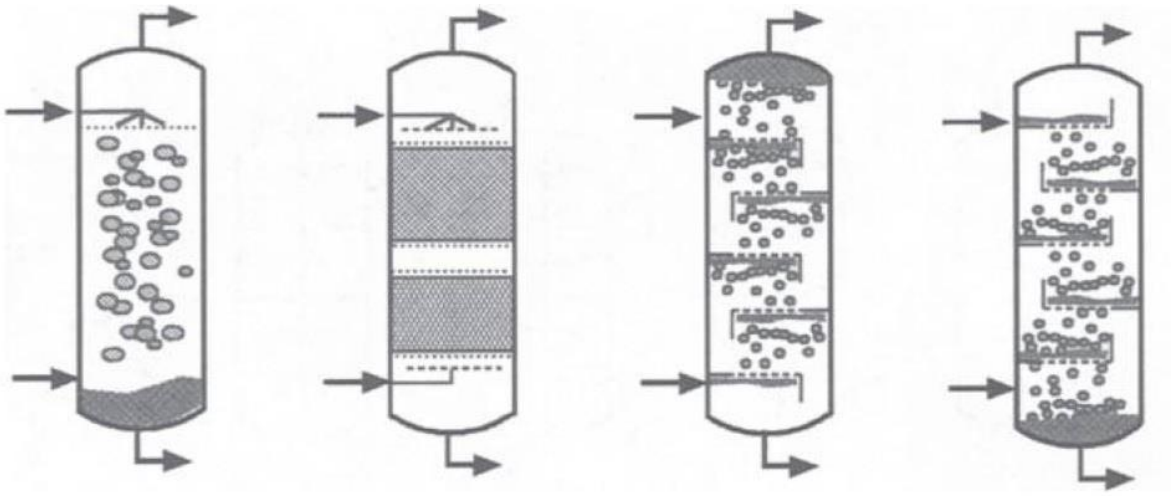

Fig. 1. Different types of non-agitated columns (from left to right: spray, packed, light sieve tray, heavy sieve tray) [2].

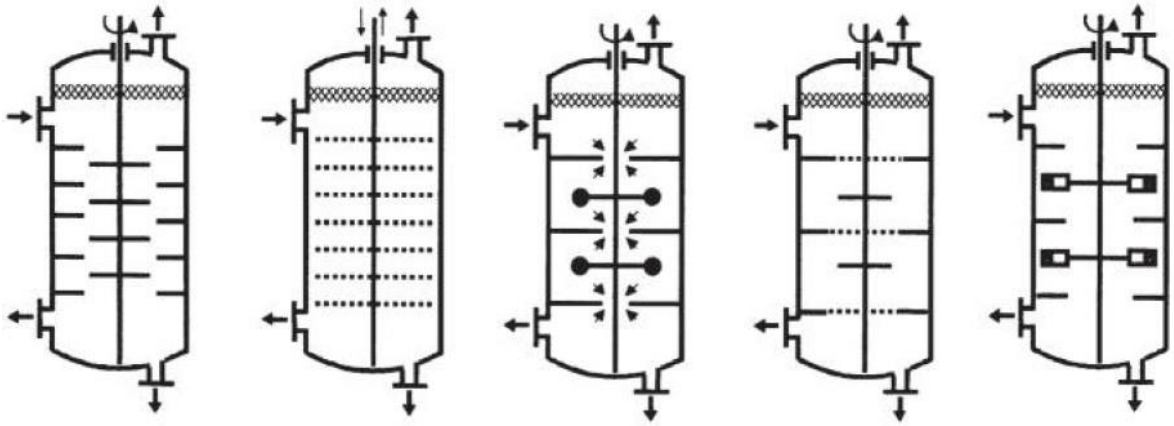

Fig. 2. Different types of agitated extractors (from left to right: RDC, Karr, Oldshue-Rushton, Kuhni, Scheibel extraction column) [2].

3.1 Complex formation

In general, reactive extraction can be described as following: the extractant reagent (*HA*) diffuses into the aqueous phase, where it reacts with the ion over several steps, resulting in the formation of the neutral complex (ML_n), which is then transferred back into the organic phase. This sequence was presented by Szymanovski [4] on the example of copper extraction step by step via following equations:

$$2HA_{org} \rightarrow (HA)_{2org}\ , \tag{1}$$

$$HA_{org} \rightarrow (HA)_{wat}, \tag{2}$$

$$HA_{wat} \rightarrow H^{+}_{wat} + A^{-}_{wat}, \tag{3}$$

$$Cu(H_2O)^{2+}_6 + A^{-}_{wat} \rightarrow Cu(H_2O)_4\ A^{+}_{wat} + 2H_2O \text{ (slow)}, \tag{4}$$

$$Cu(H_2O)_4\ A^{+}_{wat} \rightarrow Cu(H_2O)_2\ A^{+}_{wat} + 2H_2O, \tag{5}$$

$$Cu(H_2O)_2\ A^{+}_{wat} \rightarrow CuA_{2wat} + 2H_2O, \tag{6}$$

$$CuA_{2wat} \rightarrow CuA_{2org}. \tag{7}$$

Indexes *wat* and *org* stand for water and organic phases respectively. Generally, it was considered, that the formation of the first complex is the limiting step. However, in the seventies, it was proposed that the complex formation should be presented not as a bulk

reaction between the ligand *A* and the metal ion, but as an interfacial mechanism. So, the overall sequence could be represented as following:

$$2HA_{org} \rightarrow (HA)_{2org}\ , \tag{8}$$

$$HA_{org} \rightarrow HA_{ad} \rightarrow (HA)_{wat}, \tag{9}$$

$$Cu^{2+}_{wat} + HA_{ad} \rightarrow CuA^{+}_{ad} + H^{+}_{wat}, \tag{10}$$

$$CuA^{+}_{ad} + HA_{int.wat} \rightarrow CuA_{2ad} + H^{+}_{wat} \text{ (slow)}, \tag{11}$$

$$CuA^{+}_{ad} + HA_{ad} \rightarrow CuL_{2ad} + H^{+}_{wat} \text{ (slow)}, \tag{11a}$$

$$CuA_{2ad} \rightarrow CuA_{2org}. \tag{12}$$

Indexes *ad* and *int.wat* stand for adsorption layer and aqueous phase layer near the interface.

3.2 Interfacial activity

One of the most important parameters affecting the interfacial activity of the extractant is hydrophobicity. Almost all types of metal ion extractants possess amphiphilic character, meaning they have hydrophobic components (usually alkyl chains) as well as hydrophilic components (that are chemically active). Hydrophobicity, as well as the structure of alkyl groups, can affect the distribution of the extractant near the interface and its adsorption. Straight alkyl groups result in higher hydrophobicity of the extractant that of the one with branched alkyl groups. Also, one long alkyl group is more hydrophobic then two short ones.

As it was described by Szymanovski [4], the extractant molecule can be described as a combination of hydrophilic (H) and lipophilic (L) groups. After the adsorption between the water (W) and the organic (O) phases, ten combinations are possible: HH, HL, HW, HO, LL, LW, LO, WW, WO and OO. The adsorption efficiency is determined by the energies of the lipophilic part of the organic phase and the hydrophilic part of the water phase. If their sum is greater that the cohesive energy of all eight other parts, the extractant molecule is well adsorbed and properly oriented at the interface. If, however, the cohesive energy of the organic side is bigger than the one of the water side, the molecule is located is a less suitable position, being dragged into the organic phase.

In systems containing aromatic hydrocarbons, interactions between HH and LL parts are being neglected, but the interactions between water and aromatics OW are of greater importance. The existing interactions between aromatic hydrocarbons and the lipophilic part of extractant result in the molecules of extractant being dragged out from the aqueous layer near the interface, placing them into a less desirable position in comparison with those containing aliphatic hydrocarbons.

3.3 Reaction kinetics

The extraction reaction for copper can be expressed as the following equation:

$$Cu_{wat}^{2+} + 2HA_{org} \rightarrow CuA_{2org} + 2H_{wat}^{+}. \quad (13)$$

Reaction begins with interfacial adsorption of extractant (see equation 9), then the copper ion starts to react with the hydroxyoxime with the formation of intermediate complex (equation 10). This reaction is followed by the reaction with second hydroxyoxime molecule, resulting in full CuA_2 complex formation (see equations 11a and 11b). Due to the overall complex charge being zero, it diffuses back into the organic side (expressed by equation 12). In the water phase, several reactions take place - the association and dissociation of copper sulfate, sulfuric acid and water, described by the following equations:

$$Cu^{2+} + SO_4^{2-} \leftrightarrow CuSO_{4\,wat}, \quad (14)$$

$$H_2SO_4 \leftrightarrow HSO_4^- + H^+, \quad (15)$$

$$HSO_4^- \leftrightarrow SO_4^{2-} + H^+, \quad (16)$$

$$H_2O \leftrightarrow OH^- + H^+. \quad (17)$$

For reactions 13 – 17, the equilibrium constants will be calculated as following:

$$K_1 = \frac{[CuA_2]_{org}[H^+]^2}{[Cu]^{2+}[HA]_{org}^2}, \quad (18)$$

$$K_2 = \frac{[CuSO_4]_{wat}}{[Cu]^{2+}[SO]_4^{2-}}, \quad (19)$$

$$K_3 = \frac{[H_2SO_4]}{[HSO_4]^-[H]^+}, \quad (20)$$

$$K_4 = \frac{[HSO_4]^-}{[SO_4]^{2-}[H]^+}, \quad (21)$$

$$K_5 = [H]^+ [OH]^- . \quad (22)$$

However, because reactions 14 – 17 are way faster than copper extraction using hydroxyoxime (reaction 13), they are not taken into consideration in determination of reaction rate. The rate law, according to Tamminen *et al*[5], will be looking as following:

$$r = k[[Cu^{2+}]\frac{[HA]_{org}^2}{[H^+]} - \frac{1}{K_1}[CuA_2]_{org}[H^+]]. \quad (23)$$

Here, *k* is the pseudohomogeneous kinetic constant.

The reaction can be characterized by mass and charge balance equations as well. The mass balance for copper can be expressed via the following equation:

$$[CuSO_4]_0\chi_{wat} = ([Cu^{2+}] + [CuSO_4])\chi_{wat} + [CuA_2]\chi_{org}, \quad (24)$$

where χ stand for the volume fraction.

The mass balance for sulphur can be expressed like this:

$$[CuSO_4]_0 + [H_2SO_4]_0 = [CuSO_4] + [SO_4^{2-}] + [HSO_4^-] + [H_2SO_4], \quad (25)$$

while the hydrogen balance can be shown in the following form:

$$2[H_2SO_4]_0 + 2\frac{B}{\chi_{wat}} = [H^+] + [HSO_4^-] + 2[H_2SO_4]_{wat}, \quad (26)$$

where *B* is the concentration difference of copper due to the mass transfer from water phase into organic phase:

$$B = \left([Cu]_{wat,0} - [Cu]_{wat}\right)(\chi_{wat}) = \left([Cu]_{org} - [Cu]_{org,0}\right)(\chi_{org}). \quad (27)$$

Additionally, the species contained in the aqueous phase must satisfy the balance of charged, expressed by the following equation:

$$2[Cu^{+}] + [H^{+}] = [OH^{-}] + [HSO_4^{-}] + 2[SO_4^{2-}]. \quad (28)$$

Equations 18 – 28 characterize the equilibrium of *all* the species in both the organic phase and the water phase. [5]

4 Single droplets in liquid-liquid systems

Dispersed systems, and liquid-liquid systems in particular, are based on the concept of particles being immersed into the ambient phase. They are represented in a great variety of industrial applications, where the main goals are to achieve the extraction of a specific component or phase separation. While looking not very difficult as a general concept, real liquid-liquid extraction systems are controlled by a great number of parameters, which makes understanding their behavior quite a difficult task. To ease the task of describing the processes taking place, such systems are usually simplified to single droplets, and the mechanisms applying to one single droplet are extended on the whole process later on. Usually these are divided into two branches: fluid dynamics and mass transfer.

4.1 Fluid dynamics

4.1.1 General description

Because the process of liquid-liquid extraction involves two phases in constant contact with each other, the behavior of the particle will be affected by the properties of the dispersed phase as well as of the continuous phase, most important ones being: densities and viscosities of both phases, droplet diameter and interfacial tension. While describing the fluid dynamic behavior, two extreme conditions can be introduced: rigid particles with an immobile surface and particles with a fully mobile surface. The difference between them is that the first ones have zero tangential velocities and the interface, while the second ones have some specific tangential velocity at the interface, resulting in internal circulations.

The general balance of the particle can be described with the following equation:

$$F_i + F_G + F_B + F_{C_D} = 0\ , \tag{29}$$

where $F_i=M_P(dv_p/dt)$ is the inertia force, $F_G=M_pg$ is the gravitational force, $F_B=g\rho_cV_p$ is the buoyancy force, and $F_{C_D} = C_D(\frac{\rho_C}{2})v_p^2A_p$ is the drag force. C_D here stands for the drag coefficient, which can be calculated with the use of the next formula:

$$C_D = \frac{24}{Re}\frac{\frac{2}{3}+\mu^*}{1+\mu^*}, \quad (30)$$

where $\mu^*=\mu_d/\mu_c$ is the viscosity ratio.

It should be mentioned, however, that this equation, derived by Hadamard and Rybczynski [6], has some limitations. It is only applicable for small Reynolds numbers (Re<<1), with no analytical solution for higher Reynolds numbers available. Moreover, the overall behavior of the drag coefficient – decreasing with the Reynolds number increasing – remains only until the particle is spherical in shape. With liquid particles dispersed in the liquid continuous phase, however, some deviations from ideal spherical shape are possible due to the mobility of the interface. The deformation of the droplet causes an increased projected surface, and, as a result, greater drag. This creates the need to define the flow modes and the extreme conditions that separate them.

4.1.2 Regimes of flow

The droplets size range can be separated by the behavior of the droplet's interface into three parts: the *spherical* regime, where the velocity increases with the diameter, the *oscillatory* regime, where the velocity decreases with the diameter, and the *transition* regime separating the two, where the velocity reaches a peak and then starts to decrease.

In the spherical regime, the drag coefficient for rigid particles C_D is a function of the Reynolds number *Re* and the density ratio ρ^*. The mobile interface of liquid particle is taken into consideration by introducing the viscosity ratio μ^* into the equations. However, Feng and Michaelides [7] have proven that the effect of the density ratio is negligibly small, so it is generally not included into the calculation. In the end, in the spherical mode the calculation of the drag coefficient is performed using equation (30).

At some point of value of the droplet diameter, which is usually called the peak diameter d_{peak}, the droplet reaches its critical velocity v_{peak}. This velocity is the maximum velocity the droplet can achieve in the given conditions, while the drag coefficient at this moment is at minimum. Increasing the velocity will result into entering the transition mode, where the velocity no longer increases, oscillations start taking place, the surface area becomes

dependent of the frequency of oscillation, which complicates the mass transfer characteristics. The moment of transition can be defined by the dimensionless Weber number using the following equation:

$$We_{cr} = \frac{v_t^2 d_p \rho_c}{\gamma}. \tag{31}$$

The transition can be easily seen in Figure 3, representing the results of the experiments carried out by Wegener *et al* [8].

The critical value of the Weber number is 4. Beyond it, the drag coefficient calculation has to be performed using the following equation:

$$C_D = \frac{MoRe^4}{48} \text{ [7]}, \tag{32}$$

where *Mo* is the Morton number:

$$Mo = \frac{g\mu_c^2 \Delta\rho}{\rho_c^2 \gamma^3}. \tag{33}$$

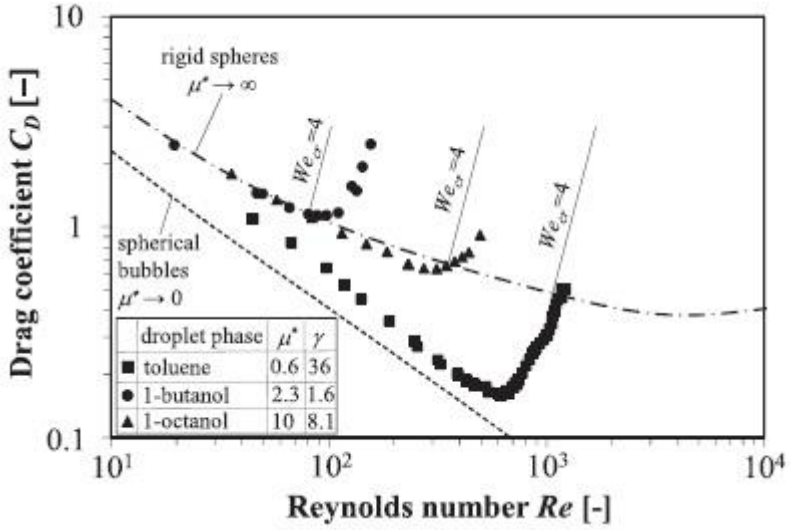

Fig. 3. Drag coefficients as a function of Reynolds number for three different systems [8].

Eventually, the droplets deforms more and more and can reach a point of oscillating in a periodic manner, where the drag coefficient can be calculated as following:

$$C_D = \frac{4}{3} MoRe^4 We^{-3}, \tag{34}$$

and droplets with larger diameters can start wobbling, undergoing aperiodic shape deformations.

4.1.3 Terminal velocity

The equation for calculating the terminal velocity of the droplet can be derived from the balance of forces affection the droplet, expressed by equation (29). In the case of unsteady particle the terminal velocity will be represented as following:

$$\frac{dv_p}{dt} = \frac{|\Delta\rho|}{\rho_d + \kappa\rho_c} g - \frac{3}{4} C_D \frac{\rho_c}{\rho_d + \kappa\rho_c} \frac{v_p^2}{d_p} . \tag{35}$$

κ is the coefficient stands for the volume fraction of the accelerated ambient fluid by the particle. It only plays a role when the phases accelerate relative to each other, so it should be taken into consideration at the stage where the particle accelerates to its terminal velocity. For rigid particles, it is equal to 0.5, however different researchers report a wide range of values for liquid particles in liquid continuous phase. For the steady-state condition though the unsteady terms can be neglected, so the equation is transformed into the following form:

$$v_t = \sqrt{\frac{4}{3} \frac{|\rho_d - \rho_c|}{\rho_c} g d_p \frac{1}{C_D}} . \tag{36}$$

As it was stated before, these correlations are only applicable with Weber number not increasing the value of 4, thus droplet keeping its spherical shape.

4.2 Mass transfer

4.2.1 General description

The main parameter describing the mass transfer process in the Sherwood number. There is a great number of equations that can be used to calculate it depending on other parameters, however, the common expression for it is the following:

$$Sh_c = \frac{\beta_c d_p}{D_{A,c}} . \tag{37}$$

β_c is the continuous mass transfer coefficient, determined by the next equation, illustrated by Figure 4:

$$\dot{m}_A = \beta(c_{A,I} - c_{Ac,\infty}). \tag{38}$$

In the simplest case of a stagnant droplet in a steady state the mass transfer is driven by diffusion and the Sherwood number will be equal to 2 [8]. Real processes, however, are much more complicated, being moving droplets with mobile interfaces. To classify these, the partition coefficient K^* is introduced, and together with the diffusivity coefficients it helps to break the mass transfer processes into groups based on the resistance:

- $K^*\sqrt{(D_{A,d}/D_{A,c}} \gg 1$ – the resistance is in the continuous phase;
- $K^*\sqrt{(D_{A,d}/D_{A,c}} \ll 1$ – the resistance is in the particles;
- $K^*\sqrt{(D_{A,d}/D_{A,c}} \approx 1$ – the resistance is in both phases.

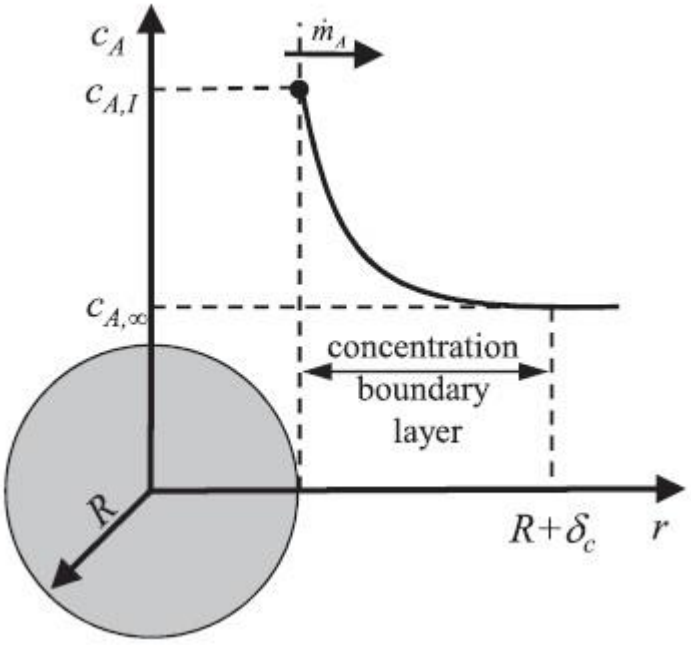

Fig. 4. Steady-state mass transfer at a droplet with an immobile interface [8]

The diffusion coefficient can be calculated from the Stokes-Einstein equation [10]:

$$D = \frac{k_B T}{6\pi\mu_c R_{0,c}}, \tag{39}$$

and assuming the same hydrodynamic radius for both phases, the ratio of diffusion coefficients can be replaced with the ratio of viscosities:

$$\frac{D_{A,d}}{D_{A,c}} \approx \frac{\mu_c}{\mu_d} = \frac{1}{\mu^*}. \tag{40}$$

This, however, is unlikely to be true for complex fluids, such as polymers. Care must be taken while replacing the ratio of diffusion coefficients with the ratio of viscosities.

4.2.2 External/internal problems

External problem is the case of having resistance in the continuous phase, while the resistance of the particles in negligibly small. The Sherwood number in this case will be determined by the Peclet number of the continuous phase (though the general assumption is that the Peclet numbers are above 100), while being at the same time dependent from the flow regime. For slow flow modes, where the Reynolds number doesn't exceed 1, the Sherwood number equals [11]:

$$Sh_c = 0.65\sqrt{\frac{Pe_c}{1+\mu^*}}. \tag{41}$$

Different correlations exist for intermediate Reynolds numbers, for example the one proposed by Thorsen [12] is valid in the range of $50 < Re < 800$:

$$Sh_c = -178 + 3.62 Re_c^{1/2} Sc_c^{1/3}. \tag{42}$$

For higher Reynolds numbers the mass transfer is happening near the interface only, so the Sherwood number is calculated the following way:

$$Sh_c = f\frac{2}{\sqrt{\pi}} Pe_c^{1/2}, \tag{43}$$

where f is the correction factor designed to take into account the correlation between the internal circulations of the particle and the Reynolds number. The relation is represented on figure 5.

Internal problem, on the other hand, occurs when the resistance lies inside the droplet, while the mass transfer is much faster in the continuous phase. In this case the mass transfer rate

doesn't depend on the partition coefficient, but the Fourier number comes into play. The dimensionless mean concentration is, as stated by Piarah [13]:

$$C^*_{A,d} = \frac{C_{A,d}(t) - K^* C_{A,c}(t\to\infty)}{C_{A,d}(t=0) - K^* C_{A,c}(t\to\infty)}. \tag{44}$$

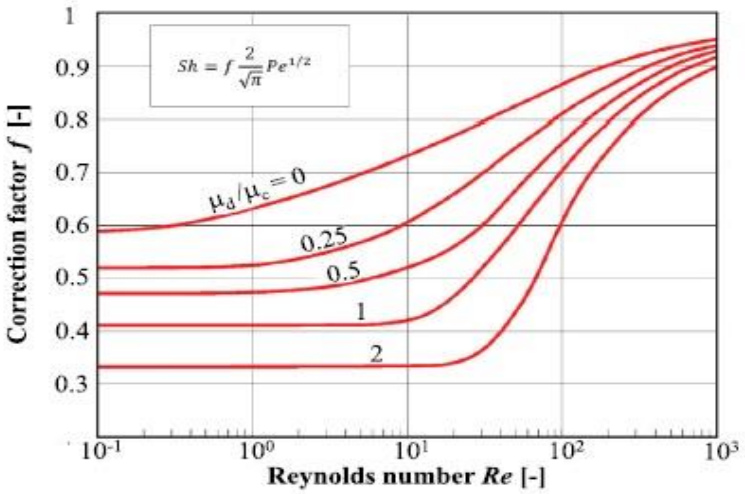

Fig. 5. Correction factor as a function of Reynolds number for different viscosity ratios [8].

The simulation results for the dimensionless mean concentration as a function of Fourier number are represented on figure 6. On this figure, low Peclet numbers represent small internal circulation (thus the mass transfer is driven by diffusion only), while high Peclet numbers stand for strong internal convection.

Figure 7 represents the values for Sherwood numbers in correlation to Fourier and Peclet numbers. On low Fourier numbers, the Sherwood number can be expressed using the following formula [8]:

$$Sh_d = \frac{4}{\sqrt{\pi}} Fo_d^{-1/2}, \tag{45}$$

while the approximated expression for mean dimensionless concentration will be:

$$c^* = \frac{6}{\sqrt{\pi}} \sqrt{\frac{4tD_{A,d}}{d_p^2}}. \tag{46}$$

So, for low Fourier numbers, the asymptotic value of the Sherwood number will be 6.58. As for the high Fourier numbers, the mean concentration will be calculated using the stream function by Hadamard, representing specific parameters B and λ [6]:

$$c^* = \frac{3}{8}\sum_{n=1}^{\infty} B_n^2 \exp(-16\lambda_n Fo_d), \tag{47}$$

resulting in the Sherwood number of 17.9.

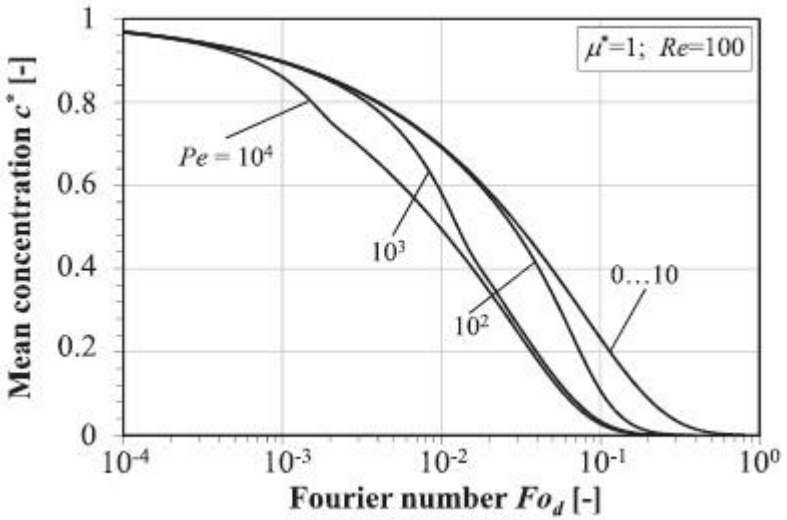

Fig. 6. Mean concentration as a function of the Fourier number for different Peclet numbers [8].

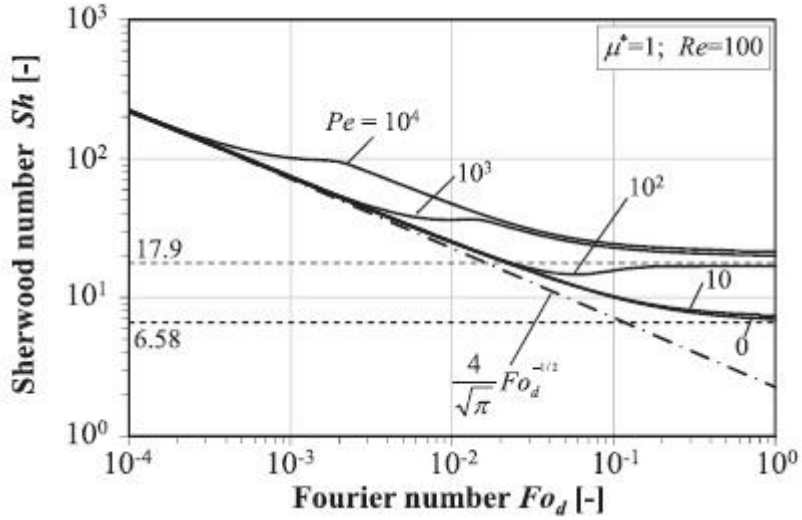

Fig. 7. Mean Sherwood number as a function of the Fourier number for different Peclet numbers [8].

Conjugate problem is a case when the resistance in both the continuous and the dispersed phases is more or less the same. With both convection and diffusion involved, the description of the process is a lot more complicated, since the concentration changes along the particle surface. Generally, no analytical solutions for these conditions exist. One possible approach is to utilize the addition rule from the film theory that can be expressed by the following equation:

$$\frac{1}{k_0} = \frac{1}{\beta_d} + \frac{K^*}{\beta_c}, \tag{48}$$

which includes both the resistance inside the particles $\frac{1}{\beta_d}$ and the resistance in the continuous phase $\frac{K^*}{\beta_c}$.

4.2.3 Marangoni convections and internal circulations

As it was mentioned above, in the case of conjugate problem, when the resistance lies in both liquid phases, the distribution of the concentration along the surface of the particle could be uneven. This can lead to the creation of so-called Marangoni circulations. The concentration distribution results in complex internal circulations that in the end result in correlation between the concentration field and the flow pattern of the particle. These correlations can have a significant effect on the mass transfer rate, but at the same time they can be extremely difficult to describe. The basic patterns of Marangoni convections are shown on figure 8.

Extensive experiments were performed by Wegener *et al* [14] on the topic of Marangoni convections and their effect on overall mass transfer. In these experiments, toluene was used as a dispersed phase and water was used as a continuous phase. The general pattern of droplet behavior achieved was the following: after detaching from the nozzle, the droplet accelerated to a specific velocity that was lower that the terminal velocity expected for those specific droplet sizes and chemicals. The Marangoni convections present inside the droplets were creating tangential shear forces, resulting in interfacial convection directed opposite to the external flow. Obviously, it created additional drag and reduced the speeds relative to the

ones expected from the droplets. As mass transfer occurs, the concentration difference in the droplet and the continuous phase was decreasing, which resulted in Marangoni convections starting to weaken after some time. Interfacial convection, as a consequence, was decreasing, which made it possible for internal circulation to start developing, and the droplets started to accelerate again to the velocities much closer to terminal ones. If the initial concentration, however, was very small, the Marangoni convections were not big enough to slow the droplet down, so the droplet accelerated to its terminal velocity from the start. The graphs representing both ways of behavior are shown in figure 9.

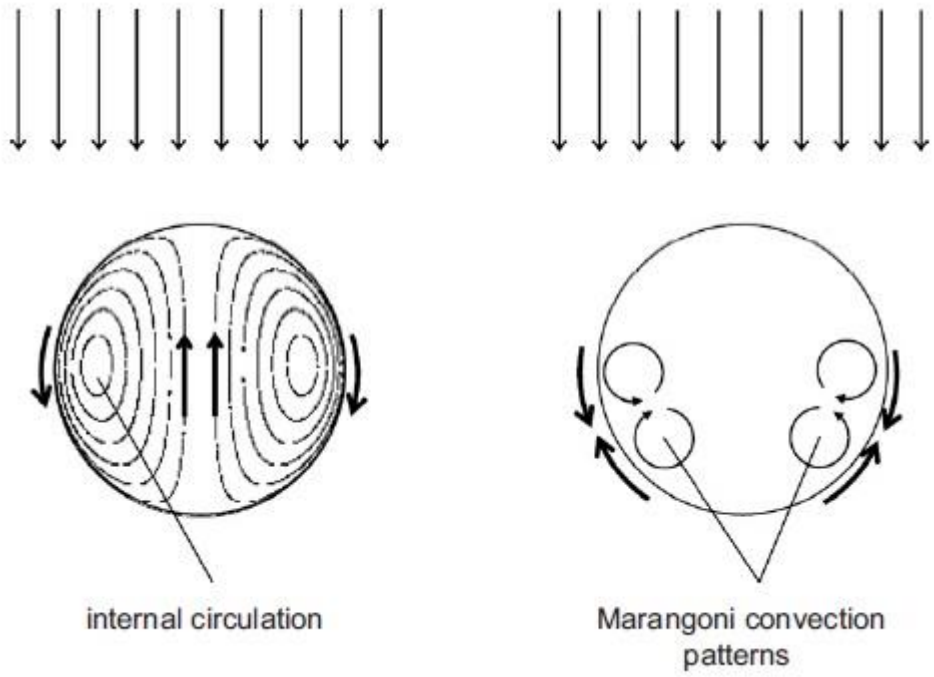

Fig. 8. Droplet with internal toroidal circulations (left), formation of internal Marangoni convection (right).

In the end, the main consequence can be described as following: the droplet velocity becomes the function of droplet concentration. This results in mass transfer depending on Reynolds and Peclet numbers, which increase the mass transfer coefficient the greater they are. The effect of retardation leads to decreased mass transfer. However, internal mixing inside the droplet can lead to improvements in mass transfer. This can be demonstrated by figure 10. It represents the time necessary to achieve 50% of mass transfer completed. In the left part of the curve (c_A < 0.1 g/L), the concentration is relatively small, so Marangoni

convections don't develop in full scale. The droplet can accelerate to its terminal velocity with Reynolds numbers being high. This is the case when the process is dominated by internal circulations. In between c_A = 0.1 g/L and c_A = 1.8 g/L, the Marangoni circulations start to occur. This results in higher drag and a lower Reynolds number. However, the Marangoni circulations are not strong enough to be able to compensate the decrease of Reynolds number, so the time to complete 50% of the mass transfer increases. After that, the Marangoni convections grow more and more powerful, which improves internal radial mixing, lowering internal resistance. The problem becomes an external one, with resistance lying in the continuous phase.

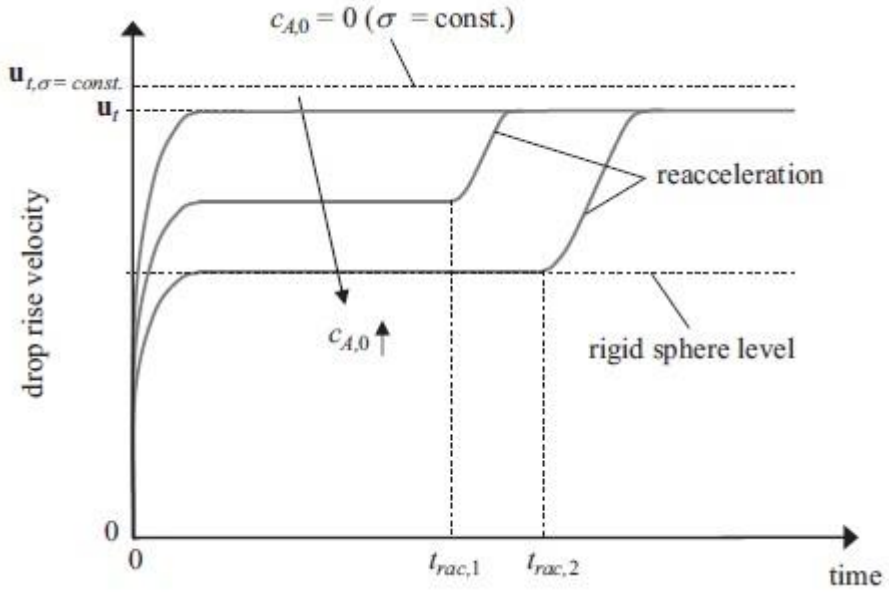

Fig. 9. Two-step acceleration due to Marangoni convections [14].

All these correlations, however, are extremely complicated, so while an extensive work has been done in the field of researching Marangoni convections, there is still no analytical solution that can describe them.

4.3 Additional factors

These factors can be of great variety: different impurities, surfactants, etc. The presence of additional particles on the interface can have a significant effect on the mass transfer, because it will define the level of mobility of the interface – from rigid-like particle immobile surface to fully mobile one, creating an influence on the velocity the droplet can achieve. However, the task to determine the degree of contamination is extremely difficult. Even if the concentrations of added impurities/surfactants are known, there still may be additional impurities provided by the chemicals used as the dispersed/continuous phases, the equipment used in the experimental setup. To be able to determine these parameters, the results of experiments using perfectly clean equipment should be available, which is almost impossible. However, using the combination of experiments and computational fluid dynamics (CFD) modelling looks like a promising mechanism of solving such a task.

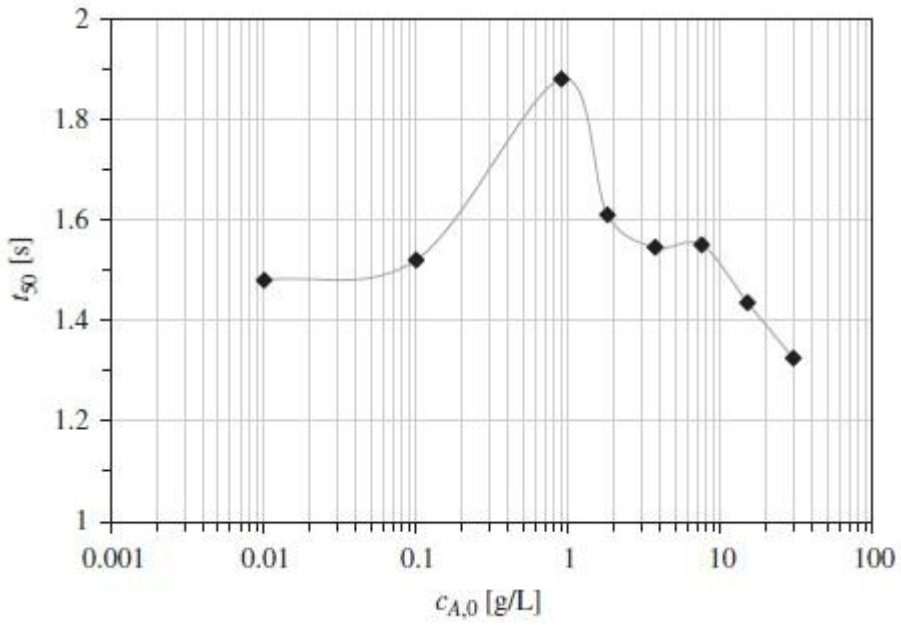

Fig. 10. Simulated time t_{50} as a function of initial solute concentration [14].

5 Single droplet experimental setup

5.1 Different setups

Generally, the setups used in single droplet experiments are more or less similar to each other. The main differences come from the phases used (replacing the water phase with organic one and vice versa will result in the change of the direction of the particle movement), the materials and shape of the column, as well as the equipment used to feed the solutions into the column. As an example, a setup used by Wegener *et al* [15] is represented in figure 11.

In this setup, a cylindrical column (1), equipped with a jacket (2), is used to perform the experiments. The jacket is filled with anhydrous glycerol that helps to minimize the distortion caused by the cylindrical shape of the column. A pump (4) and a thermostat (5) are used to keep the glycerol circulating through the jacket to maintain the constant temperature. The dispersed phase is contained in the tank (3a) and is delivered into the column via a syringe pump (7a). In order to be able to form a particle of a specific size on the tip of the nozzle (6), a solenoid (8) controlled by a computer (12a) is used. The continuous phase is prepared in a stirred tank (9). The particle formed by the nozzle travels through the column into the funnel (11), where it is withdrawn by another syringe pump (7b) into a tank (3b), and later the collected sample concentration is analyzed using the gas chromatograph (GC). A computer-controlled (12b) high speed camera (10) is filming the particles at the rate of 50 – 350 frames per second, which gives the opportunity for very fine particle rise velocity estimation.

This setup, however, has a limitation in possible residence time. Theoretically, the reverse of the direction of the continuous phase circulation (so the droplet rise and the continuous phase flow will be counter-current) can help to achieve greater residence times, but the increased relative velocity can result in droplets going into transition or oscillatory regime of flow, ruining the experiment. In order to avoid this, Venturi tubes are used, as described by Bart and Stevens [2]. The principle of the setup is shown on Figure 12.

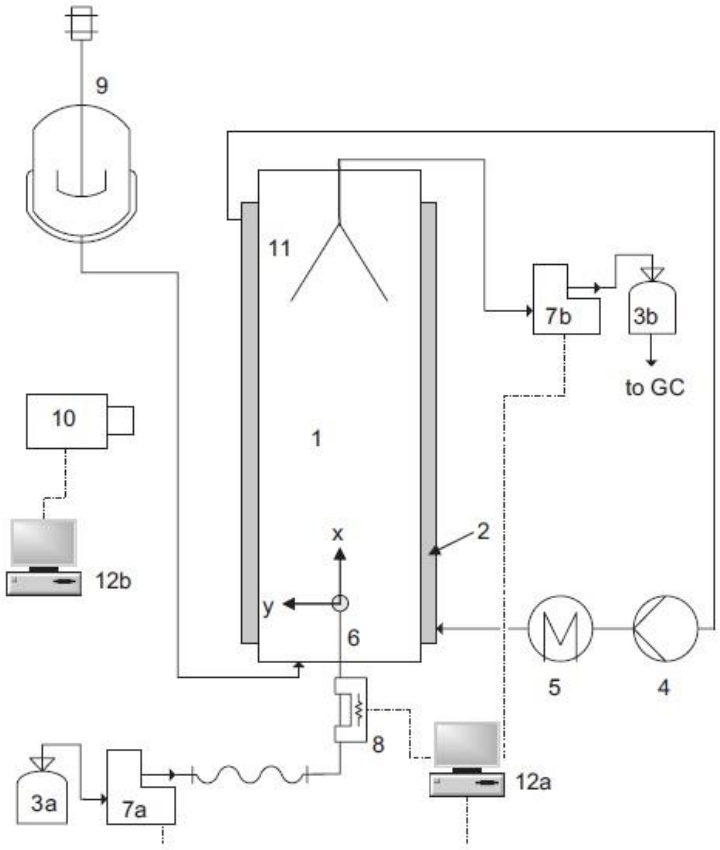

Fig. 11. Experimental setup for velocity and concentration measurements of single rising droplets [15].

The basic principle remains the same: the dispersed phase is delivered to the nozzle (3) from the storage tank (1) via the metering pump (3). The gear pump (4) is used to control the droplet diameter at the moment of its detachment from the nozzle, while the circulating pump (5) and the heat exchanger (6) provide the counter-current flow of the continuous phase at a constant temperature. The released droplets are collected using the funnel (7) and then extracted for further analysis (8). The valve (9) is used to adjust the flow of the continuous phase, so that the droplets can be kept inside the Venturi tube for a necessary period of time.

The same concept of filming droplets flowing through the continuous phase in a glass tube was used by Kamp and Kraume [16] while performing the experiments on droplet coalescence in liquid-liquid systems. The general layout is shown on Figure 11. The oil pump (1) fitted with a three-port valve was used to deliver specific amounts of oil for upper

and lower droplets. The water pump (2) was used to deliver the remaining oil form the T-fitting (4) to the cannula and release the droplet. The volume of the water used to create a pulse for droplet detachment was carefully controlled to avoid unnecessary additional acceleration. The collision of the droplets was filmed by a high-speed camera (5) with the assistance of backlighting provided by the LED flash (6). The thermostat (7) and the thermometer (8) were busy keeping the temperature constant. The second water pump (3) was used to remove possible residues of the organic material from the upper cannula.

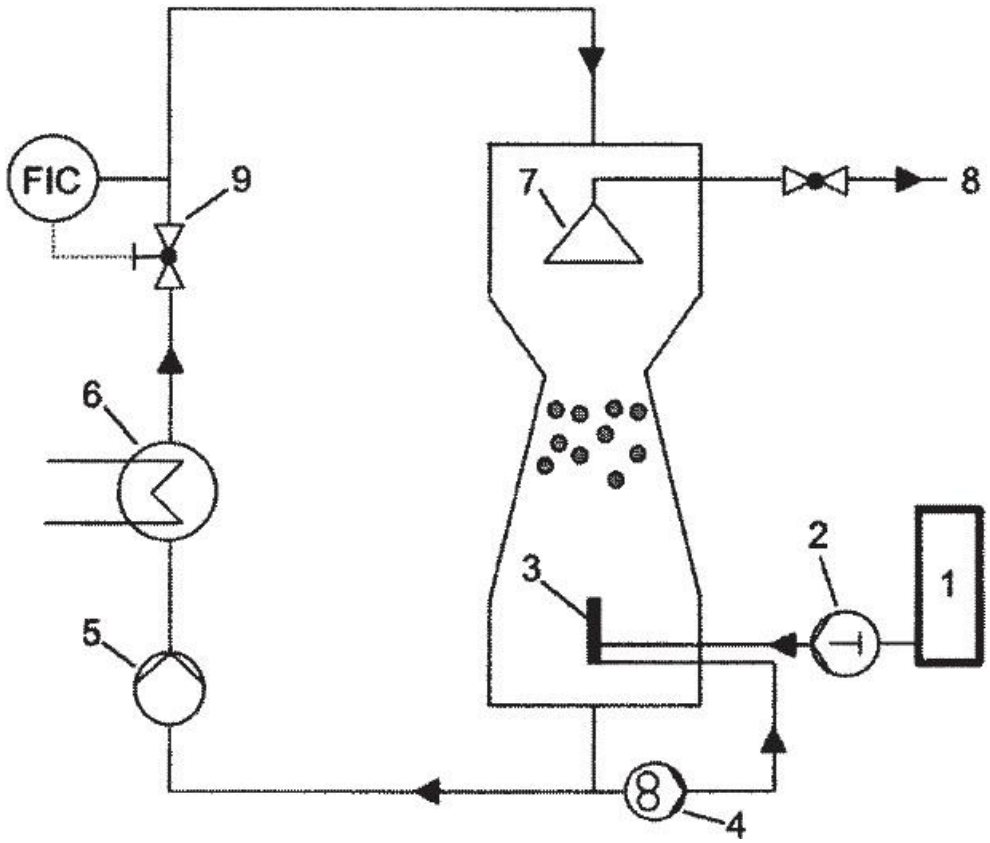

Fig. 12. Venturi tube experimental setup [2].

All the examples above, however, refer to non-agitated reactive extraction process, but, as it was mentioned in Chapter 3, different kinds of agitated extractors exist. Of course, these were not left out of the question by researches. For example, Bart [17] describes the stirring cell that was during the determination of kinetic parameters of mass transfer in stirred columns (Figure 12). There, the organic phase was fed from a tank (1) into the upper section of the column, while the water phase was fed from another tank (2) into the bottom. The valve (8) was fitted in order to empty the stirrer column from the waste after the experiments

were completed. Two ports (6 and 7) were used to collect samples. The heating jacket (3) was connected to the thermostat (4) to provide constant temperatures. The mixing itself was done by two stirrers (5) driven by electric motors (M). The rotational speed was adjustable, which helped to determine the existence of different zones:

- below 80 RPM, the mass transfer is limited by diffusional resistance;
- between 80 and 160 RPM, the mass transfer is independent of stirring;
- above 160 RPM, the disruption of the interface happens, which increases the area of the mass transfer and improves the mass transfer rate.

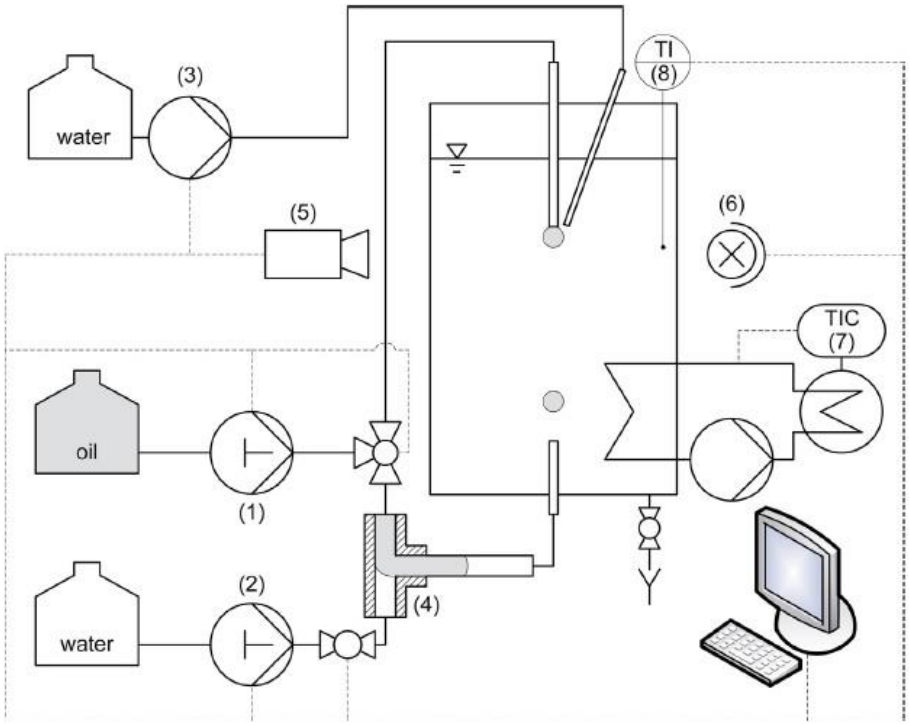

Fig. 11. Experimental setup for droplet coalescence experiments [16].

5.2 Droplet formation, settling and coalescence

Some studies show that up to 60% of mass transfer happens during droplet formation. However, performing experiments on droplet formation was proven to be problematic due to short times and small sizes. Moreover, the mass transfer during the coalescence stage is

unknown due to lack of experimental data. Generally, overall mass transfer is, that involves mass transfer during formation, rise/fall through the column and coalescence. To minimize the effect of unknown parameters, it is generally proposed to use short travel columns with surfaces as small as possible for coalescence. And yet, a decent model representing mass transfer during droplet formation is highly desirable, due to the highest concentration differences. Moreover, it is possible that the previously described Marangoni effects are present during the droplet formation phase at high concentrations. The total mass transferred, assuming the uniformity of the growing spherical droplet, can be expressed via an equation proposed by Popovich *et al.* [18]:

$$M_S = const \cdot d_{p,f}^2 \Delta c_s (D_s \pi t_f)^2. \tag{49}$$

Const in this equation is a constant which varies a lot in different sources – from 6/7 to 24/7. If the Marangoni convections are to be taken into account, the diffusivity factor α is introduced into equation (49):

$$M_S = \frac{6}{7} \cdot d_{p,f}^2 \Delta c_s (\alpha D_s \pi t_f)^2. \tag{50}$$

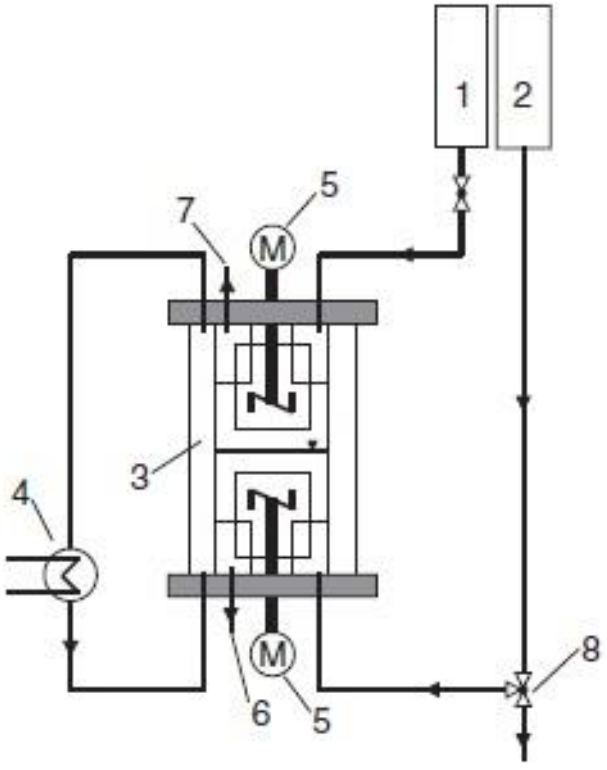

Fig. 12. Experimental setup of a stirring cell [17]

6 Experiments

6.1 Experimental setup

The general concept of the experimental setup is very similar to the ones previously described and is represented on Figure 13. The column (1) is a glass tube, rectangular in cross-section, with approximately 45 mm wide sides. During the experiments, two different columns were used – the short column has 345 mm of droplet fall distance, while the long one has 700 mm of droplet fall distance. All other dimensions of both columns are the same. To feed the dispersed phase into the column, a two-piston HPLC pump (2) was used. The type of pump that could be used in this particular setup is not restricted to HPLC pumps – for example, during the preparation for the experiments a syringe pump was tested. However, it was the two-piston HPLC pump with digital controls that was chosen due to its stability of federate, ease of operation and ability to adjust the parameters with great precision (for example, the federate can be adjusted with 0.001 ml/min precision). The dispersed phase was put into a tank (3), the pump input hose was placed inside the tank and the pump was started. Before running the actual experiments, it was run for about 10-15 minutes to displace all the water that was inside it. The pump was never left idle with actual continuous phase inside for extended periods of time to avoid crystallization of copper sulfate, and after every set of experiments, the input hose of the pump was placed into a different tank containing distilled water, so that the copper sulfate solution could be replaced with it.

The column was filled with the continuous phase using a second pump (4). The tank (5) containing Acorga M5460, diluted with Exxsol D80, which was used as the organic phase was placed on the same height as the column itself to ease the start of the procedure. However, because this pump was non-reversible, the tank was placed lower than the column to empty it after the experiment was completed. During the experiment itself, the input hose was fixed on a stand and closed airtight to avoid spills and keep the level of the continuous phase in the column stable.

The droplets were formed at the tip of the needle (6). The needles used were conventional syringe needles, with diameters of 0.4 mm, 0.5 mm, 0.6 mm, 0.7 mm, 0.8 mm, 0.9 mm and

1.2 mm. After the droplet detached from the needle, it spent several seconds falling through the column and then landed inside the funnel (7). The valve fitted at the bottom of it was used to collect the sample of the dispersed phase. Before the beginning of each experiment, the funnel was filled with dispersed phase using a glass tube to keep the continuous phase from getting into the funnel and mixing with the sample. During the experiment itself, the level of the dispersed phase in the funnel was kept low enough to minimize area of contact with the continuous phase and thus minimize the potential mass transfer yet high enough to keep the continuous phase from getting into the samples.

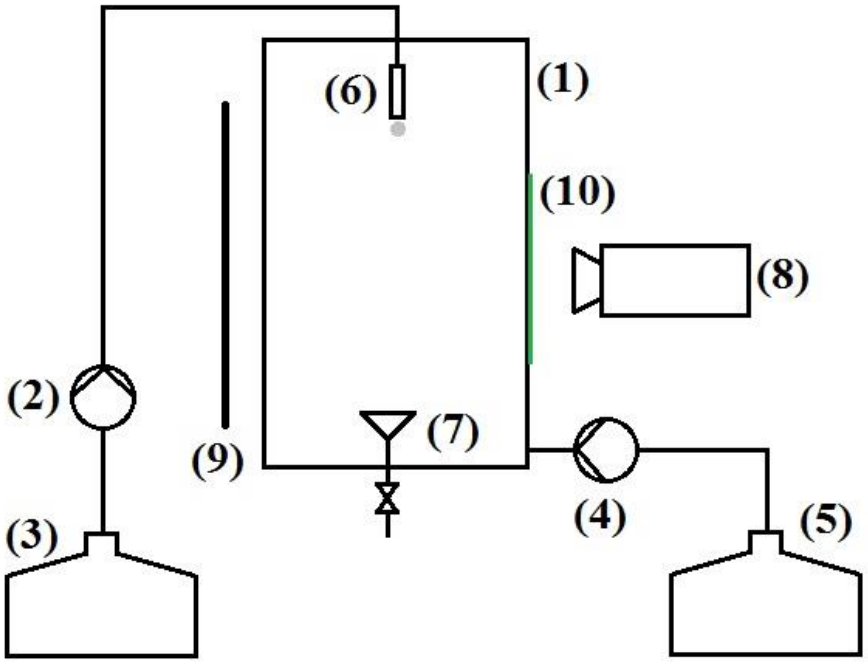

Fig. 13. General schematics of the experimental setup

The droplets falling through the column were filmed using the camera (8). It was filming at Full HD resolution (1920 x 1080 pixels) and 50 frames per second, which proved to be enough for further analysis. Behind the column, opposite to the camera, a black background (9) was placed. During the preparations for the experiments, different conditions were tested to improve the performance of the camera, such as back lighting of various colors, lighting from the sides of the column etc. However, the best results were achieved with the black

background behind the column, no additional lighting and the main lights in the laboratory shut. The lights in the laboratory itself didn't affect the quality of the video made by the camera directly, but if someone or something was moving behind the camera (especially if it was colored in white or bright colors, e.g. laboratory coat), the glass surface was reflecting it directly into the camera, making droplet recognition much more complicated. When the lights in the laboratory were shut down, the reflections form the glass column surface were minimized, improving the quality of the video. In order to perform the droplet velocity calculations, a special grid was printed on a transparent film and attached to the wall of the column (10).

The general sequence of the experiment was the following: first, the pump feeding the dispersed phase was prepared. The funnel was filled with the same phase and then attached to the bottom of the column. The mass of the material fed into the funnel was noted. Then, the column was filled with the continuous phase. The experiment itself started at the moment the level of the continuous phase reached the top of the funnel – it was the moment the two phases contacted for the first time. At this very second, the stopwatch was started. The column was filled to the level 1.5 -2 cm higher than the tip of the needle. After that, the pump feeding the continuous phase was stopped, the input hose was sealed and fix at an elevated position to avoid backflow. Then, the HPLC pump was started. Once the first droplet appeared, the specific time was noted to further calculated the feeding time. It was taking about 2 minutes to fill the short column and about 3 minutes to fill the long one. The feeding time was approximately 20 minutes for each experiments, slightly varying from one experiment to the other. During the experiment, the sample was collected into glass vessels form the funnel using the valve. After the time was up and the pump was stopped, the rest of the sample was accurately collected to avoid getting the continuous phase in the vessel. Then, the tank for the continuous phase was placed lower that the column to empty it. After the column was emptied, the funnel and the valve was cleaned with ethanol to get rid of any organic material left on it, and the setup was ready for another experiment.

It should also be mentioned, that both columns used during the experiments were designed to function in two different positions: with the funnel at the bottom – for experiments with droplets falling – and the funnel at the top – for the experiments with droplets rising. The general procedure remains the same, except the fact that with droplets rising no seed solution

is added to the funnel before the experiment was started, and the samples were collected using a pipette without the valve.

6.2 Analytics

After the experiments were complete, several parameters were determined to be able to get final results. The first parameter was the concentration of copper. It was determined for all the samples as well as feed solutions using a Cary 8454 UV-Visible spectroscopy system produced by Agilent Technologies. Before the analysis could be performed, a 3 mole sulfuric acid was prepared to dilute the samples. For those experiments where copper sulfate was acting as a dispersed phase, the ratio of 20:1 between sulfuric acid and the sample was chosen. It provided stable results during measurements and, due to the low volume of sample required, gave an opportunity to perform additional measurements if they were required. However, for those experiments where the dispersed phase was organic, it was necessary to extract copper from it into the sulfuric acid avoiding getting the organic into the sample. To do so, the organic was mixed with 3 mole sulfuric acid in small vessels and then left for several hours. After that time, the heavier acid was at the bottom of the vessel, while the organic was above it. The sulfuric acid containing copper was extracted from the vessels using syringes with 40 μm filters attached, otherwise the organic phase could have ruined the measurements due to the extreme sensitivity of the equipment. It took several attempts to determine the optimal ratio between the sulfuric acid and the organic phase sample – high ratios like 20:1 or 10:1 weren't providing consistent results, while 1:1 ratio couldn't provide enough volume of sulfuric acid to be analyzed. In the end, the ratio of 2.5:1 proved to be of an optimal balance.

Between the measurements, as well as before the first one, the sample cell was flushed with sulfuric acid that didn't contain any copper. That was done to ensure that no additional copper could get from one sample to another ruining the measurement. The calibration curve was based on the measurements of copper and 3 mole sulfuric acid with concentrations from 100 ppm to 1000 ppm, providing big enough range. The Agilent Cary 8454 system proved to be very precise, yet stable during the measurement process if the equipment was kept clean and the measurements were performed according the instructions. Sometimes, however, the performance of the system was affected by the sunlight – because it is an

optical-based system that uses two lamps (a tungsten lamp and a deuterium lamp), direct light hitting the sensor and interfering with the light from the lamps can result in completely nonsensical results. To avoid the risk of measurements being ruined in such a manner, the analysis was never performed at times when direct sunlight was breaking through window.

The density of all the samples, feed solutions and continuous phases was measured using a density meter produced by Anton Paar. The sample was fed inside the machine using a syringe, and the measurement itself was completely automatic. To ensure the precision, any bubbles in the samples should have been avoided, and the density meter was washed with pure water between the measurements and dried with air. The density meter proved to be very precise, providing an accuracy of three decimal places.

The number of droplets, as well as their velocity, was calculated via a specifically created Matlab program. The program was designed to detect the differences between consecutive frames and to determine if these differences were caused by the moving droplets. In order to get the program working, the videos were uploaded into a determined folder. Then, it was necessary to highlight the areas of droplet calculation and the reference grid. The grid was used by the program as a sample of distance – knowing the actual size of the grid and the number of pixels it was taking on the screen, the program was able to convert the number of pixels travelled by the droplet into the distance, and knowing the number of frames it took the droplet to travel that very distance as well as the fixed value of frames per second (which was 50), the program could make calculations of the velocities of every droplet and then get an average value of that. A screenshot of the video, showing a section of the grid attached to the column, as well as a part of the column without the grid, can be seen on Figure 14.

It should be noted, that the calculation of the droplets was performed by the program at the upper part of the column, where the grid doesn't obscure the view of the droplet. The grid itself was only used as a scale reference to calculate the distance and, in the end, the velocity of the droplets. Also, by looking at the screenshot, it could seem that the droplet was deforming during the fall through the column, which is not true – in reality the droplet was maintaining its completely spherical shape through the whole distance from the needle tip down to the funnel. Additionally, the glares from the film that the grid was printed on that are visible on the screenshot could never be calculated by the program as droplets by a

mistake – since the program detects the differences between the frames travelling vertically through several consecutive frames in a row, and the glares were not moving at all.

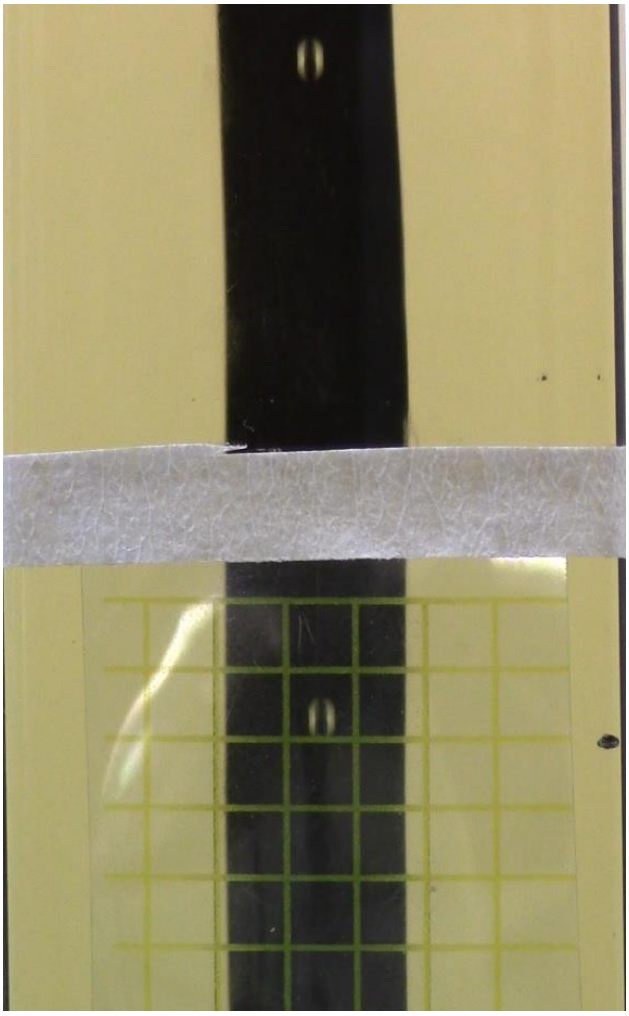

Fig. 14. A screenshot of the column with the reference grid

The program showed great performance while calculation the droplets of different sizes travelling at a wide range of speeds – from 50 mm/s up to 120 mm/s. During the experimental part of this Master's Thesis, the program was updated several times to improve its efficiency.

6.3 Experimental plan

During the experiments, the following data was collected:

- *Sample tare mass.* It was measured two times – before the experiment and after the experiment with the dispersed phase sample in it. The difference between these two values gives the mass of the sample collected;

- *Seed mass.* Before the experiment was started, the funnel was filled with the dispersed phase. The masses of the syringe used in this process before and after were measured to be able to calculate the actual mass of the solution in the funnel later;

- *Experiment time.* The timer was started, when the continuous phase got in contact with the seed solution in the funnel. The time the dispersed phase was started to be fed through the needle was indicated, as well as the ending of the feeding process. The difference between those two values gives the feeding time;

- *Concentrations.* The concentrations of copper in all the collected samples as well as in the feed solution were carefully measured. Though it was supposed that the concentrations of the feed solution would remain the same through different experiments, the actual values varied;

- *Densities.* The densities of the feed solution and all the samples were measured to be able to calculate the required volumes later on. Also, the densities of the continuous phase were measured as well;

- *The number of droplets, their velocities and diameters.* The videos of the experiments were analyzed by the software to calculate the amount of droplets fed during each experiment as well as the average velocities of their fall through the column. The diameters were estimated from the videos, as well as back-calculated from mass balance.

The variables of the experiments were the following:

- *Needle diameter.* Though not being adjustable on the fly, the change of the needle can result in different droplet size, affecting the velocity of the droplets and the surface area per unit volume *;*

- *Feedrate*. The parameter that determines the size of the droplet and, as a result, its velocity and surface area. Though it was possible to adjust this parameter during the experiment, the opposite thing was desired, as the stability of the federate meant the ability to properly determine a number of other parameters depending from it*;*

- *Copper sulfate concentration.* For the experiments, two concentrations were chosen – 0.13 M $CuSO_4$ as a higher one and 0.05 M $CuSO_4$ as a lower one, though precise values were fluctuating*;*

- *Organic phase concentration.* The organic extractant Acorga M5460 was diluted with Exxsol D80 solvent to achieve 3 different concentrations – 0.4 M, 0.2 M and 0.1 M. Most of the time, the highest concentration was used, however, during the experiments with the long column, lower concentrations were applied more extensively*;*

- *Column height.* The actual height was not adjustable – the column simply was replaced. However, with two times difference in height, the effect of such a change on the droplet travel time is unquestionable;

- *Phase inversion.* As it was mentioned before, the columns were design to functions in two positions, allowing two types of experiments: the first one with the heavier dispersed phase, where the droplets are falling, and the second one with the heavier continuous phase, where the droplets are rising.

During the experiments, different combinations of these parameters were tried out. They are briefly described in Table 1. Though the main adjustable parameter was the feedrate, sometimes additional changes were made to achieve greater variety in the data, like taking two different needle diameters or different organic phase concentrations.

It should be additionally mentioned, that sets A through J use copper sulfate water solution as a dispersed phase and Acorga M5460/Exxsol D80 solution as a continuous phase, but experiments in set K were performed with inverted phases – the water phase was continuous, and the droplets were organic. Because of that, to initial seed solution was added in the beginning of the experiment into the funnel, since it was located not at the bottom of the column, but on the top of it, and the droplets were rising upwards.

All experimental data is represented in Appendixes I and II. Tables in Appendix I have the data on initial seed and final sample masses, as well as the times of start and finish of droplet feeding. Tables in Appendix II shown the measured densities and concentrations of the feed solutions and the collected samples.

Table 1. Different combinations of variable parameters in experimental sets

Set	Copper concentration, mol/l	Acorga concentration, mol/l	Column height, mm	Needle diameter, mm	Continuous phase	Dispersed phase
A	0.15	0.4	345	0.4 and 1.2	Organic	Aqueous
B	0.13	0.4	345	0.4 and 1.2	Organic	Aqueous
C	0.044	0.4	345	0.4 and 1.2	Organic	Aqueous
D	0.151	0.4	345	1.2	Organic	Aqueous
E	0.162	0.4	345	1.2	Organic	Aqueous
F	0.142	0.4	345	1.2	Organic	Aqueous
G	0.162	0.4	700	1.2	Organic	Aqueous
H	0.162	0.2	700	1.2	Organic	Aqueous
I	0.162	0.1	700	1.2	Organic	Aqueous
J	0.16	0.4 and 0.1	345	1.2	Organic	Aqueous
K	0.155 and 0.06	0.4	345	0.4 and 1.2	Aqueous	Organic

7 Results and discussions

In order to estimate the contribution of resistances in the organic and the aqueous phases, the following equations can be used:

$$\Delta_c = \frac{1/k_c}{1/k_o}, \tag{51}$$

$$\Delta_d = \frac{1/k_d \cdot K^*}{1/k_o}, \tag{52}$$

$$\Delta_r = \frac{\frac{1}{k_o} - (\frac{1}{k_d} \cdot K^* + \frac{1}{k_c})}{1/k_o}, \tag{53}$$

where Δ_c, Δ_d and Δ_r are fractional resistances in continuous phases, dispersed phase and due to the reaction, respectfully.

Mass transfer coefficients in continuous and aqueous phases can be determined from the Sherwood number equations [20]:

$$Sh_c = \frac{k_c d_{32}}{D_c}, \tag{54}$$

$$Sh_d = \frac{k_d d_{32}}{D_d}, \tag{55}$$

where d_{32} is the Sauter mean droplet diameter, estimated by the following correlation:

$$d_{32} = \frac{\sum n_i d_i^3}{\sum n_i d_i^2}, \tag{56}$$

where n_i is the number of droplets with diameter d_i.

The Sherwood number for the continuous phase can be calculated from the equation suggested by Kumar and Hartland[19]:

$$\frac{Sh_c - Sh_{c,r}}{Sh_{c,\infty} - Sh_c} = C_2 Re^{n_1} {Sc_c}^{n_2} \left(\frac{\nu \cdot \mu_c}{\gamma}\right)^{n_3} \frac{1}{1+\mu^{*n_4}}, \tag{57}$$

where $Sh_{c,r}$ is the rigid droplet Sherwood number, calculated as following:

$$Sh_{c,r} = 2.43 + 0.775 \cdot Re^{\frac{1}{2}} \cdot Sc_c^{\frac{1}{3}} + 0.0103 \cdot Re \cdot Sc_c^{\frac{1}{3}}, \quad (58)$$

$Sh_{c,\infty}$ is the upper limit Sherwood number:

$$Sh_{c,\infty} = \frac{2}{\sqrt{\pi}} Pe_c^{1/2}, \quad (59)$$

$C_2 = 5.26 \cdot 10^{-2}$, $n_1 = 1/3 + 6.59 \cdot 10^{-2}$, $n_2 = 1/3$, $n_3 = 1/3$, $n_4 = 1.1$ and Sc_c is the continuous phase Schmidt number calculated by the next formula:

$$Sc_c = \frac{\mu_c}{\rho_c D_c}. \quad (60)$$

The continuous phase Reynolds and Peclet numbers are derived from the following equations:

$$Re_c = \frac{d_{32} v \rho_c}{\mu_c}, \quad (61)$$

$$Pe_c = \frac{d_{32} v}{D_c}. \quad (62)$$

The dispersed phase Sherwood number is calculated using the next equation [20]:

$$Sh_d = 17.7 + \frac{a \cdot \left(Re \cdot Sc_d^{1/3}\right)^{1.7}}{1 + b \cdot \left(Re \cdot Sc_d^{1/3}\right)^{0.7}} \cdot \rho^{*2/3} \cdot \frac{1}{1 + \mu^{*2/3}}, \quad (63)$$

where $a = 3.19 \cdot 10^{-3}$, $b = 1.43 \cdot 10^{-2}$.

The overall mass transfer coefficient can be calculated from the following equation:

$$\dot{F_{Cu}} = k_0 \cdot ([\mathrm{CuA_2}]^* - [\mathrm{CuA_2}]), \quad (64)$$

where $\dot{F_{Cu}}$ is the copper ion flux, $[\mathrm{CuA_2}]^*$ and $[\mathrm{CuA_2}]$ are molar copper complex equilibrium concentration and molar copper complex bulk concentration, respectfully. Because the bulk concentration is negligibly low, we can calculate the overall mass transfer coefficient as following:

$$k_0 = \frac{\dot{F_{Cu}}}{[\mathrm{CuA_2}]^*}. \quad (65)$$

$[\mathrm{CuA_2}]^*$ is the concentration in balance with the copper concentration , $[\mathrm{Cu}^{2+}]$. They are related via the partition coefficient:

$$K^* = \frac{[\mathrm{CuA_2}]^*}{[\mathrm{Cu^{2+}}]}, \tag{66}$$

that is also required in Eqs. (52) and (53). It can be calculated by using the next equation:

$$K^* = K_e \frac{[\mathrm{HA}]^2}{[\mathrm{H^+}]^2}, \tag{67}$$

where K_e is the equilibrium constant, $K_e = 15$ [21], [HA] is final Acorga concentration, $[\mathrm{H^+}]$ is final proton concentration.

Final Acorga concentration is calculated in the next way:

$$[\mathrm{HA}] = [\mathrm{HA}]_o - \frac{2 \cdot \dot{F_{Cu}}}{k_{HA}}, \tag{68}$$

where $[\mathrm{HA}]_o$ is the initial Acorga concentration and k_{HA} is the film mass transfer coefficient.

The equation for final proton concentration is the following:

$$[\mathrm{H^+}] = \frac{V \cdot [\mathrm{H^+}]_0 + 2 \cdot \dot{F_{Cu}} \cdot A}{V}, \tag{69}$$

where $[\mathrm{H^+}]_0$ is the initial proton concentration, *A* is the droplet surface area.

During the calculations, the following constant values were used:

- $D_c = 0.29 \cdot 10^{-9}$ m^2/s;
- $D_{Cu} = 0.72 \cdot 10^{-9}$ m^2/s;
- $\gamma = 30 \cdot 10^{-3}$ N/m;
- $\mu_{aq} = 0.9$ mPa·s;
- $\mu_{org} = 1.2$ mPa·s;

The results of mass transfer coefficients calculations are represented in Appendix III.

In order to simplify the analysis of the results, they were divided into several groups based on the similarity of the conditions. Excluding all variables but one from the sets made it easier to show what kind of effect – if there was any – that specific variable had on the results. The full list of experimental conditions is represented in Table 1 (see Section 6.3).

- Group 1 conditions were the following: needle diameter – 1.2 mm, high Acorga M5640 organic phase concentration – 0.4 mol/l, high copper concentration in aqueous phase (ranging from 0.162 to 0.13 mol/l). Experiments done both in short (345 mm) and long (700 mm) travel columns are present. This group includes: experiments 4-6 from Set A, experiments 4-6 from Set B, Sets D, E, F, G and experiment 6 from Set J;
- Group 2 conditions differed in the needle diameter, which was 0.4 mm, the high Acorga M5640 concentration (0.4 mol/l) and high copper concentration (0.13 – 0.15 mol/l) remain. The column travel was 345 mm. This group includes: experiments 1-3 from Set A, experiments 1-3 from Set B;
- Group 3 includes the experiments from Set C, which was performed using both 0.4 and 1.2 mm needle, high Acorga concentration (0.4 mol/l), but the copper concentration in the aqueous phase was lower – 0.044 mol/l. Column travel was 345 mm;
- Group 4 incudes the experiments from Set K, in which the needle diameters were varied (0.4 and 1.2 mm), as well as the copper concentration (0.06 and 0.155 mol/l). High Acorga concentration was used (0.4 mol/l), and the column travel was 345 mm. The difference is that the phases were inverted – the copper aqueous solution was the dispersed phase, while the organic solution was used as the continuous phase.

Figures 15 – 18 show the correlation between mass transfer rate and the feedrate for these groups.

As it can be seen from the graphs, the mass transfer rate increases with the feedrate. However, the values depend on variable conditions – the mass transfer rate will be bigger, if the needle diameter is greater, the copper sulfate concentration is higher, though the column length doesn't affect the mass transfer rates at all. For inverted phase conditions, when organic droplets are rising through the aqueous phase, neither needle diameters nor copper sulfate concentrations plays a significant role in affecting the mass transfer rate, though the overall tendency to increase with the feedrate remains the same.

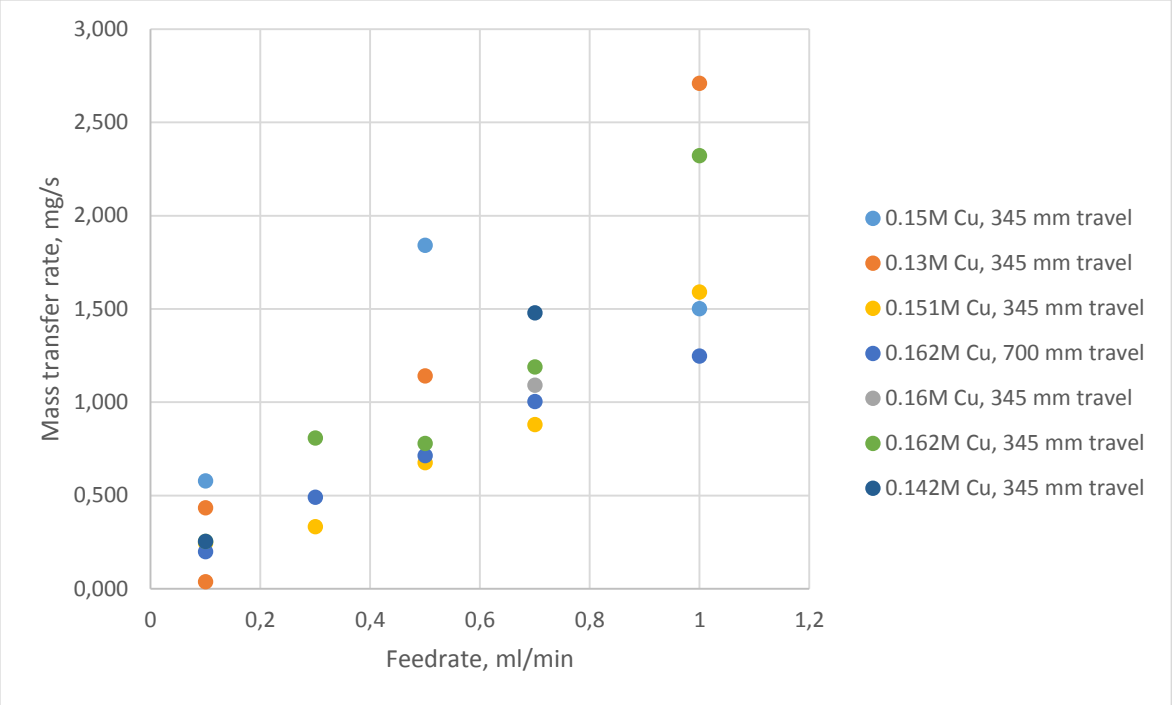

Fig. 15. Mass transfer rates at different feedrates for different copper concentrations and column travel lenghts. Experimental conditions: needle diameter – 1.2 mm, Acorga concentration – 0.4 mol/l, $CuSO_4$ water solution as dispersed phase.

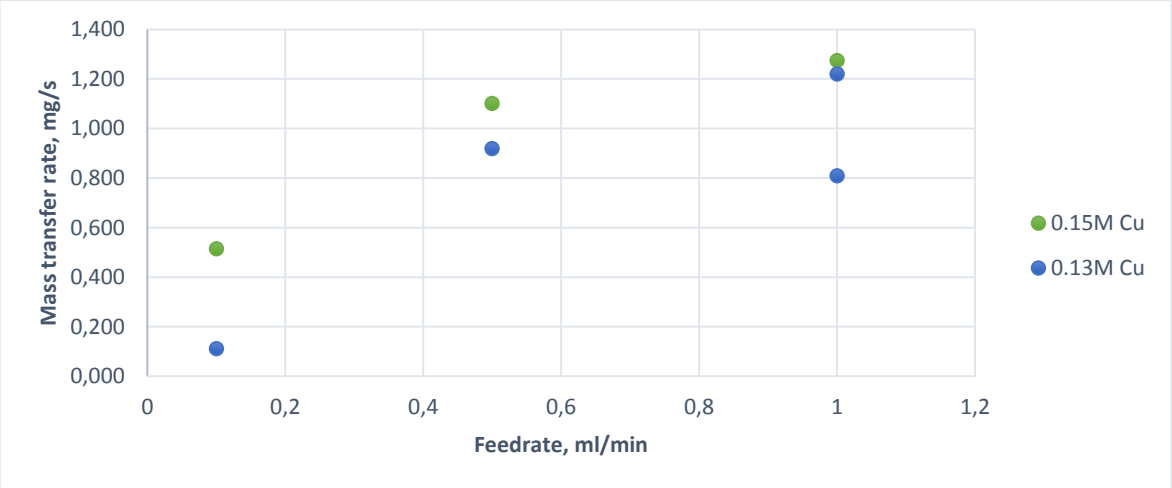

Fig. 16. Mass transfer rates at different feedrates for different copper concentrations. Experimental conditions: needle diameter – 0.4 mm, Acorga concentration – 0.4 mol/l, column travel length – 345 mm, $CuSO_4$ water solution as dispersed phase.

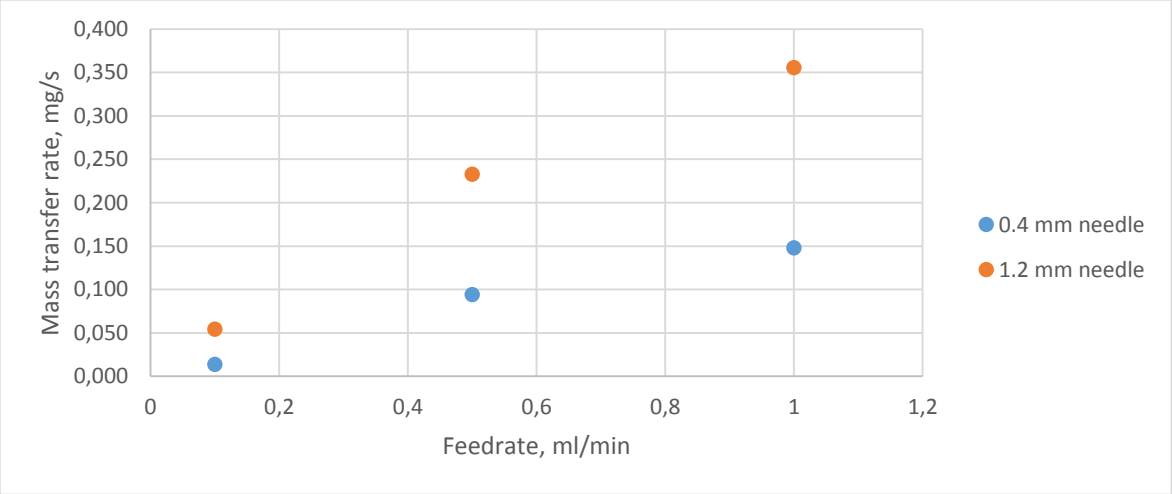

Fig. 17. Mass transfer rates at different feedrates for different needle diameters. Experimental conditions: Acorga concentration – 0.4 mol/l, copper concentration – 0.044 mol/l, column travel length – 345 mm, $CuSO_4$ water solution as dispersed phase.

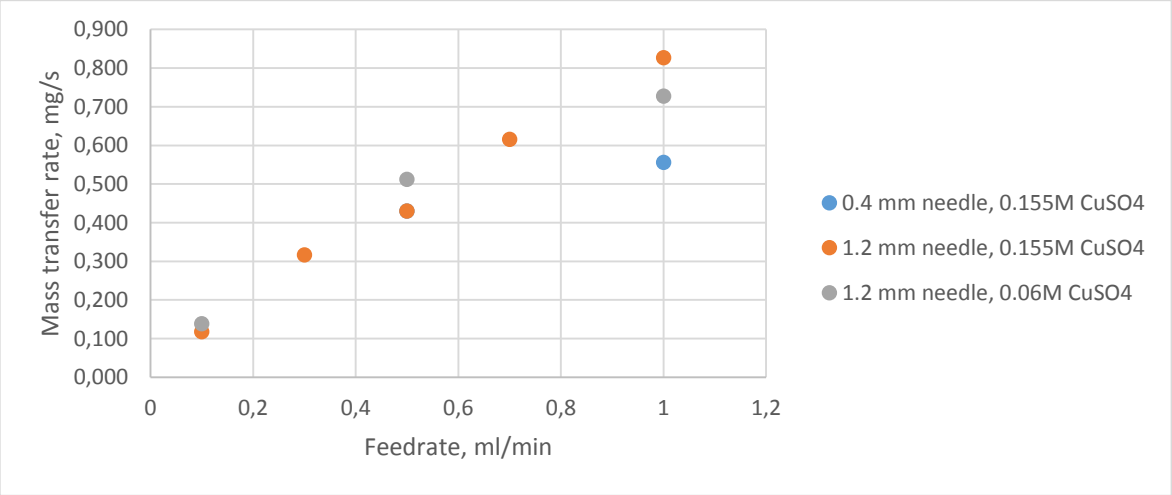

Fig. 18. Mass transfer rates at different feedrates for different needle diameters and copper concentrations. Experimental conditions: Acorga concentration – 0.4 mol/l, column travel length – 345 mm, $CuSO_4$ water solution as continuous phase.

The graphs representing the fractional resistances at different feedrates are shown on figures 19 – 22, the values of fractional resistances are provided in tables 2 - 5.

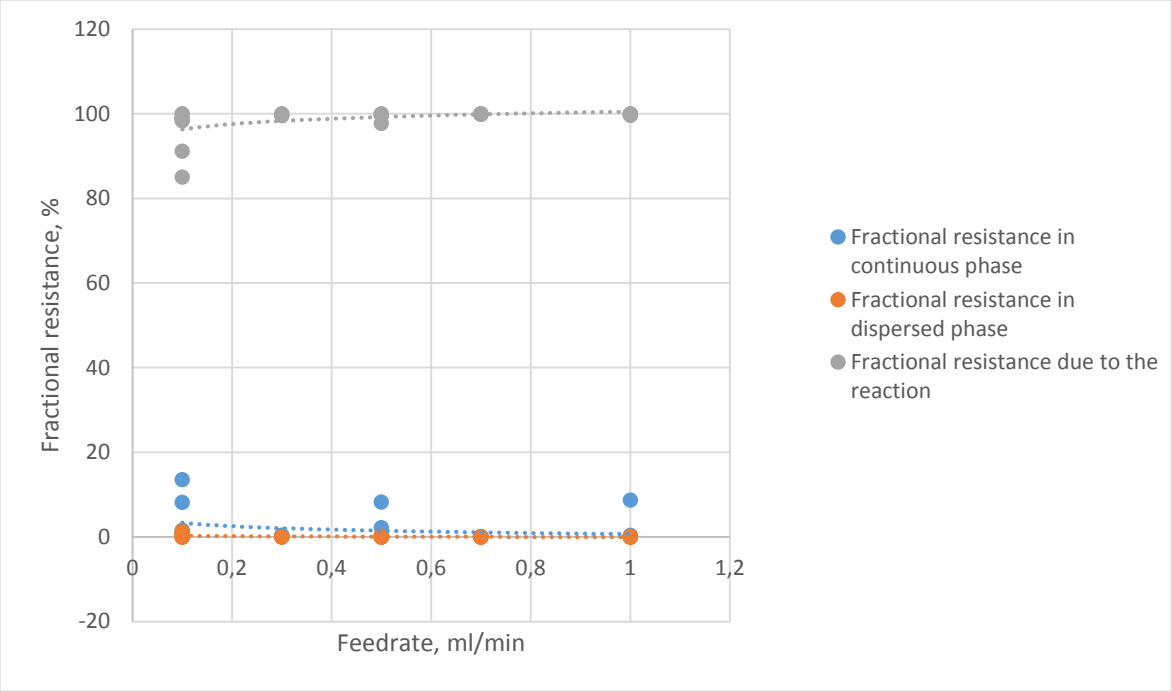

Fig. 19. Fractional resistances at different feedrates for different copper concentrations and column travel lengths. Experimental conditions: needle diameter – 1.2 mm, Acorga concentration – 0.4 mol/l, copper concentration – 0.13 – 0.162 mol/l, 345 and 700 mm column travel lengths, $CuSO_4$ water solution as dispersed phase.

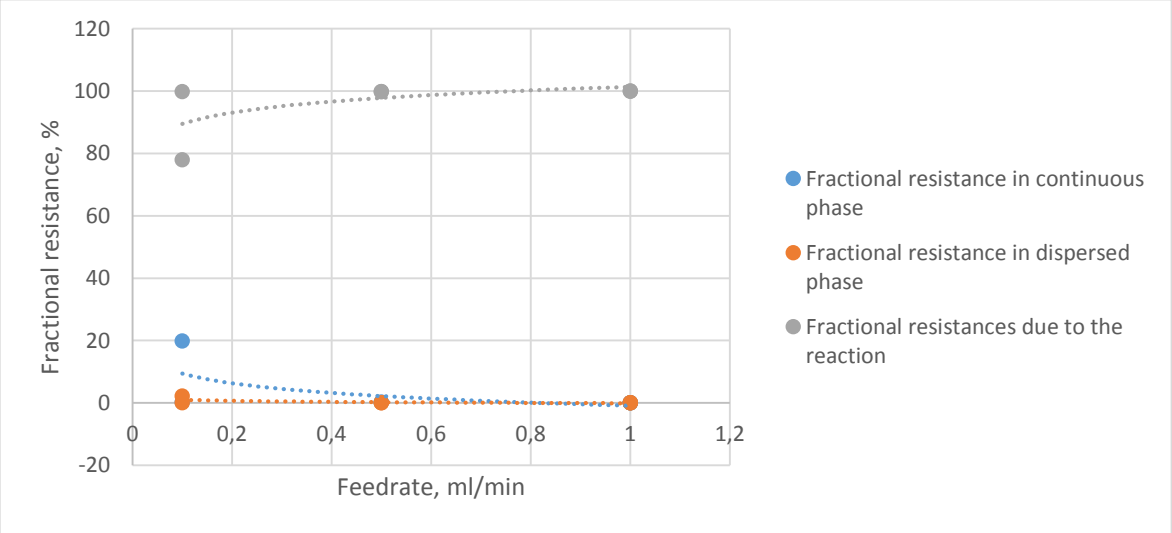

Fig. 20. Fractional resistances at different feedrates for different copper concentrations and column travel lengths. Experimental conditions: needle diameter – 0.4 mm, Acorga concentration – 0.4 mol/l, copper concentration – 0.13 – 0.15 mol/l, 345 mm column travel length, $CuSO_4$ water solution as dispersed phase.

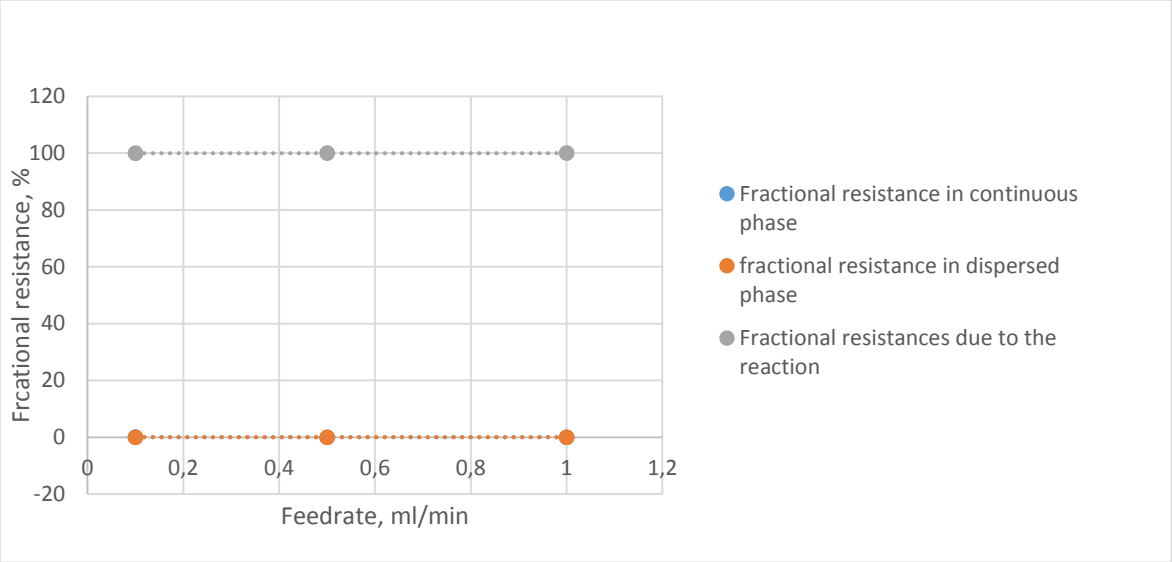

Fig. 21. Fractional resistances at different feedrates for different copper concentrations and column travel lengths. Experimental conditions: needle diameters – 0.4 and 1.2 mm, Acorga concentration – 0.4 mol/l, copper concentration – 0.044 mol/l, column travel length – 345 mm, $CuSO_4$ water solution as dispersed phase.

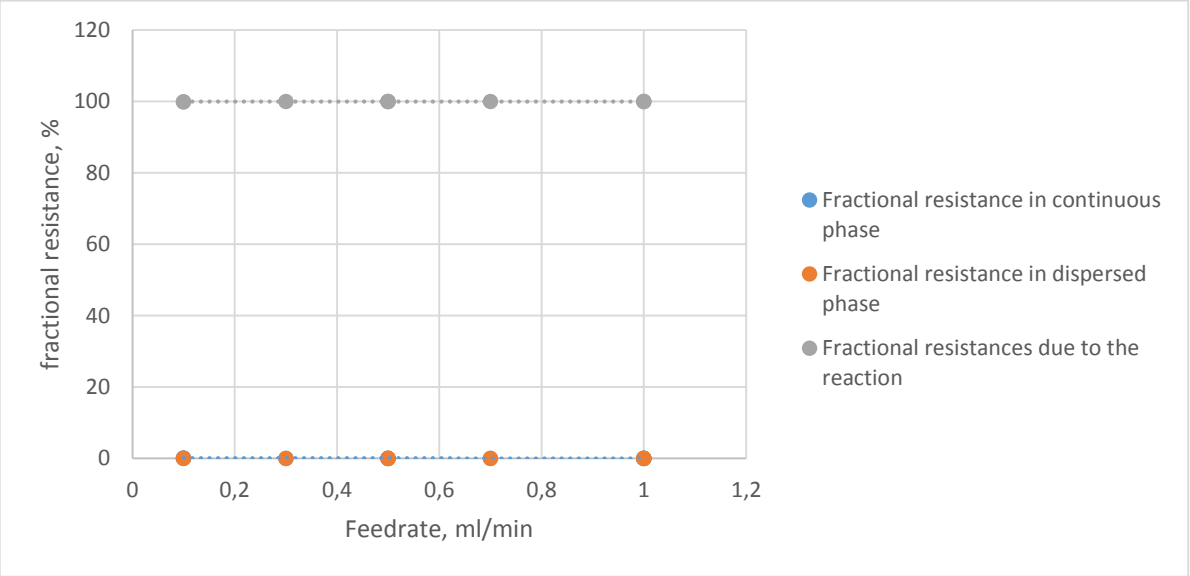

Fig. 22. Fractional resistances at different feedrates for different copper concentrations and column travel lengths. Experimental conditions: needle diameters – 0.4 and 1.2 mm, Acorga concentration – 0.4 mol/l, copper concentrations 0.06 and 0.155 mol/l, column travel length – 345 mm, $CuSO_4$ water solution as continuous phase.

Table 2. Fractional resistances for experiments with the following conditions: needle diameter – 1.2 mm, Acorga concentration – 0.4 mol/l, copper concentration – 0.13 – 0.162 mol/l, 345 and 700 mm travel column lengths, $CuSO_4$ water solution as dispersed phase.

Set	№	Fractional resistance in the continuous phase Δ_c, %	Fractional resistance in the dispersed phase Δ_d, %	Fractional resistance due to the reaction Δ_r, %
A	4	13,565	1,386	85,050
	5	2,198	0,033	97,769
	6	0,040	0,000	99,960
B	4	8,160	0,670	91,170
	5	0,313	0,001	99,686
	6	0,385	0,001	99,613
D	1	1,601	0,030	98,370
	2	0,024	0,000	99,976
	3	0,035	0,000	99,965
	4	0,020	0,000	99,980
	5	0,032	0,000	99,968
E	1	1,239	0,020	98,741
	2	0,367	0,002	99,631
	3	0,061	0,000	99,939
	4	0,051	0,000	99,949
	5	0,110	0,000	99,889
F	1	1,098	0,015	98,887
	2	85,856	11,105	3,040
	3	8,256	0,225	91,518
	4	0,111	0,000	99,889
	5	8,723	0,200	91,077
G	1	0,724	0,006	99,270
	2	0,410	0,002	99,588
	3	0,221	0,001	99,778
	4	0,097	0,000	99,903
	5	0,046	0,000	99,954
J	6	0,028	0,000	99,972

Table 3. Fractional resistances for the experiments with the following conditions: needle diameter – 0.4 mm, Acorga concentration – 0.4 mol/l, copper concentration – 0.13 – 0.15 mol/l, 345 mm column travel length, $CuSO_4$ water solution as dispersed phase.

Set	№	Fractional resistance in the continuous phase Δ_c, %	Fractional resistance in the dispersed phase Δ_d, %	Fractional resistance due to the reaction Δ_r, %
A	1	19,877	2,145	77,978
	2	0,238	0,001	99,761
	3	0,069	0,000	99,931
B	1	0,221	0,002	99,777
	2	0,157	0,001	99,843
	3	0,006	0,000	99,994

Table 4. Fractional resistances for the experiments with the following conditions: needle diameters – 0.4 and 1.2 mm, Acorga concentration – 0.4 mol/l, copper concentration – 0.044 mol/l, column travel length – 345 mm, $CuSO_4$ water solution as dispersed phase.

Set	№	Fractional resistance in the continuous phase Δ_c, %	Fractional resistance in the dispersed phase Δ_d, %	Fractional resistance due to the reaction Δ_r, %
C	1	0,002	0	99,998
	2	0,001	0	99,999
	3	0	0	100
	4	0,071	0	99,929
	5	0,009	0	99,991
	6	0,002	0	99,998

For experimental group 3 (see Fig. 21, Table 4), the values of fractional resistances in the continuous phase as well as in the dispersed phase are so small that we can assume that the whole 100% of resistance is the resistance due to the reaction itself. The same situation prevails for experimental group 4, as it can be seen from Figure 22.

Table 5. Fractional resistances for the experiments with the following conditions needle diameters – 0.4 and 1.2 mm, Acorga concentration – 0.4 mol/l, copper concentrations 0.06 and 0.155 mol/l, column travel length – 345 mm, $CuSO_4$ water solution as continuous phase.

Set	№	Fractional resistance in the continuous phase Δ_c, %	Fractional resistance in the dispersed phase Δ_d, %	Fractional resistance due to the reaction Δ_r, %
C	1	0,0189	0	99,981
	2	0,0267	0	99,973
	3	0,076	0	99,924
	4	0,016	0	99,984
	5	0,031	0	99,969
	6	0,088	0	99,912
	7	0,016	0	99,984
	8	0,019	0	99,981
		0,032	0	99,968
		0,022	0	99,978

The overall tendency for the fractional resistances is to decrease with the feedrate increment. However, several things should be pointed out: first, the values for the continuous phase resistances are in all cases bigger than the ones for the dispersed phase resistances. Secondly, the fractional resistances are bigger, when the copper sulfate concentration is bigger. And the last one is that in case of inverted phase experiments, the values of fractional resistances are so small they are almost negligible.

The behavior of the Sherwood number values is similar in all conditions – it increases with the diameter. Though there were much more experiments with 1.2 mm needle, rather than with the 0.4 needle, it can be clearly seen that the needle diameter makes little to no difference for the Sherwood number. However, the Sherwood number doesn't increase linearly – the greater the diameters, the more difference the same increment in diameters will make, as it can be seen in Figure 23. Eq. (63) shows, that there is a number of parameters, which can be assumed constant for a set of experiments, e.g. viscosities, densities, etc., but

the Reynolds number changes during the set, since it depends on the velocity, which itself depends on the droplet size. The complexity of the formula and a significant number of other parameters involved make it difficult to find a direct correlation between the diameter and the Sherwood number, but the final equation on the graph shows a 0.92 fit, which can be considered good.

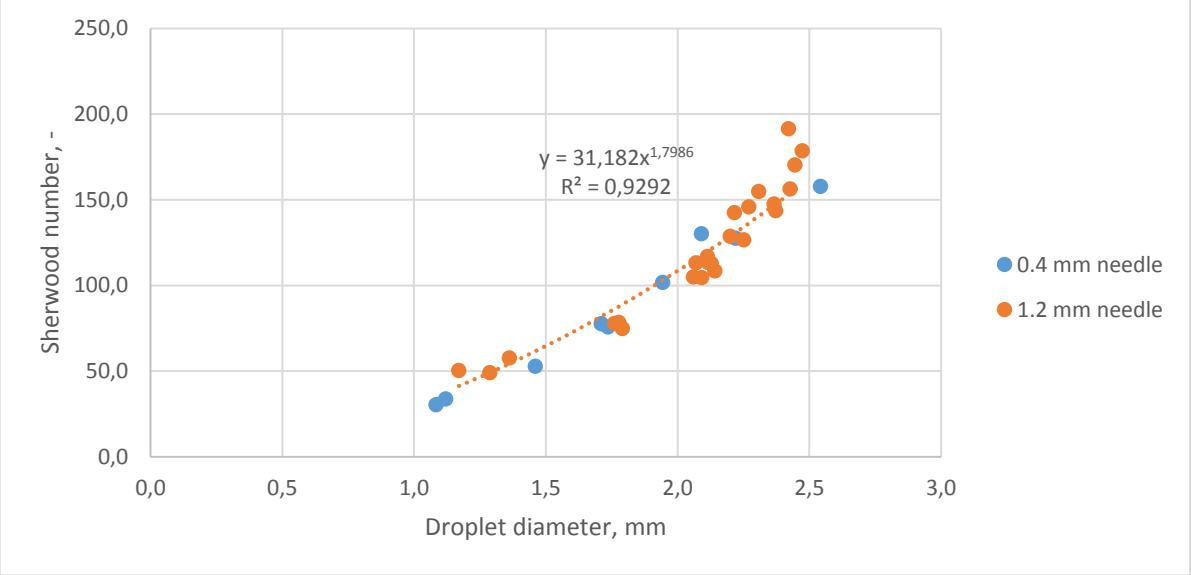

Fig. 23. Sherwood numbers at different droplet diameters

Values of Sherwood numbers for all experiments can be found in Appendix III.

Conclusions

During the experiments carried out in this Master's Thesis, the process of solvent extraction of copper via Acorga M5640 organic extractant was researched. A number of parameters have been evaluated, such as mass transfer rates and fractional resistances in relation to dispersed phase feedrates, organic and aqueous phase concentrations, column lengths and other parameters. The result is represented by figures that shown clear qualitative relations.

As it was determined, the mass transfer rate in normal phase experiments (organic solution as the continuous phase, aqueous solution as the dispersed phase) depends on the feedrate, the needle diameter as well as the concentration of the $CuSO_4$ water solution. The increased feedrate leads to the growth of the mass transfer rate values. The mass transfer rate also increases with bigger copper concentrations in the water phase. Bigger needle diameters also provide greater mass transfer rate values. However, one interesting conclusion is that the mass transfer rates are indifferent to column travel length/residence time. Increasing the column height twice didn't have any effect on the results whatsoever, considering all other parameters constant. For inverted phase experiments (organic solution as disperced phase, aqueous solution as continuous phase) neither the needle diameter not copper sulfate concentration proved to have any effect on the mass transfer rate.

The Sherwood number, as it could be expected, proved to be dependent from the droplet diameter. The correlation between these two parameters is complex, since the Sherwood number depends on the Reynolds number, which by itself depends on diameter as well as the droplet velocity, which is a function of the droplet diameter on its own. Still, the equation acquired that directly links the Sherwood number and the droplet diameter shown a good fit.

As for the resistance determination, the results show that the greatest part of it is due to the reaction itself. At high copper concentrations as well as big needle diameters the values of fractional resistances in the dispersed and the continuous phases are relatively big (up to 15% and more), but at low concentrations, as well as in case of inverted phase experiments, they become so small they are almost non-existent. These extremely high values refer to the situations where the aqueous to organic ratios are very high, and the concentration of the extractant is deficient [20].

Because of the sheer number of parameters measured during the experiments themselves, as well as the substantial volumes of calculations, the results can't be considered absolutely precise. Among the parameters that were measured, the droplet velocities and sizes could have a greater effect on imprecision, since they were measured by software which demanded some specific conditions, e.g. lighting, background contrast, threshold level adjustments. The stability of the droplet delivery by the pump was also a matter of concern – any air bubbles or impurities in the system can ruin any hopes for a constant droplet delivery and formation times. The masses measured, as well the concentrations, were less of a problem due to the simplicity of the equipment used and the procedures required to perform a measurement. Also, the lack of information and previous research on complex formation during droplet formation and coalescence, as well as a number of assumptions made during estimation of resistances of the phases to mass transfer and other speculations could have affected the quantitative estimations. Further improvements, such as elaborations of the processes taking place during droplet formation, will hopefully decrease the degree of error in future research of liquid-liquid solvent extraction behavior.

References

[1] Holmyard, E.J. 1957. Alchemy. London: Pelican Books.

[2] Bart, H., Stevens, G.W. 2004. Reactive solvent extraction.

[3] Bart, H. 2002. Reactive extraction of acids or metals—the state of the art of column design. *Chemical engineering science*, vol.57, p. 1.

[4] Szymanovski, J. 2000. Kinetics and interfacial phenomena. *Institute of Chemical Technology and Engineering, Poznan University of Technology, Poznan, Poland.*

[5] Tamminen, J., Sainio, T., Paatero, E. 2013. Intensification of metal extraction with high-shear mixing. *Lappeenranta University of Technology, Lappeenranta, Finland.*

[6] Hadamard, J.S. 1911. Mouvement permanent lent d'une sphere liquid et visqueuse dans un liquid visqueux, pp.1735-1743.

[7] Feng, Z.-G., Michaelides, E.E. 2001. Drag coefficients of viscous spheres at intermediate and high Reynolds numbers, pp. 841–849.

[8] Wegener, M., Paul, N., Kraume, M. 2014. Fluid dynamics and mass transfer at single droplets in liquid/liquid systems. *Int.J. Heat Mass Transfer,* pp.475-495.

[9] Harper, J.F. 1972. The motion of bubbles and drops through liquids. *Adv. Appl. Mech. 12*, pp. 59-129.

[10] Einstein, A. 1905. Über die von der molekularkinetischen Theorie der Wärme geforderte Bewegung von in ruhenden Flüssigkeiten suspendierten Teilchen (in German). *Ann. Phys. 17*, pp. 549–560.

[11] Lochiel, A.C., Calderbank, P.H. 1964. Mass transfer in the continuous phase around axisymmetric bodies of revolution. *Chem. Eng. Sci. 19*, pp. 471–484.

[12] Thorsen, G., Terjesen, S.G. 1968. On the mechanism of mass transfer in liquid–liquid Extractions. *Chem. Eng. Sci. 17*, pp. 137–148.

[13] Piarah, W.H. 2001. Numerische Untersuchung des instationären Stofftransports an und in umströmten Einzeltropfen (in German). Ph.D. thesis. Verlag Köster, Berlin

[14] Wegener, M., Eppinger, T., Bäumler, K., Kraume, M., Paschedag, A.R. and Bänsch, E. 2009. Transient rise velocity and mass transfer of a single drop with interfacial instabilities – numerical investigations. *Chem. Eng. Sci. 64*, pp. 4835–4845.

[15] Wegener, M., Grunig, J., Stuber, J., Kraume, M., Paschedag, A.R. and Kraume, M. 2007. Transient rise velocity and mass transfer of a single drop with interfacial instabilities –experimental investigations.

[16] Kamp, J., Kraume, M. 2014. Influence of drop size and superimposed mass transfer on coalescence in liquid/liquid dispersions – Test cell design for single drop investigations.

[17] Bart, H. 2003. Reactive extraction in stirred columns – a review.

[18] Popovich, A.T., Jervis, R.E., Trass, O. 1964. Mass transfer during single drop formation. *Chem. Eng. Sci. 19*, pp. 357–365.

[19] Kumar, A.; Hartland, S. Correlations for Prediction of Mass Transfer Coefficients in Single Drop Systems and Liquid–Liquid Extraction Columns. Chem. Eng. Res. Design 1999, 77, 372-384.

[20] Ferreira, A.E.; Agarwal, S.; Machado, R.M. *et al.* 2010. Extraction of copper from acidic leach solution with Acorga M5640 using a pulsed sieve plate column. *Hydrometallurgy 104*, pp. 66–75.

[21] Tamminen, J.; Sainio, T.; Paatero, E. 2013. Intensification of metal extraction with high-shear mixing. *Chemical Engineering and Processing 73*, pp. 119-128.

Set	№	Needle, mm	Feedrate, ml/min	Seed mass before, g	Seed mass after, g	Feed start time, min:sec	Feed finish time, min:sec	Sample tare mass before, g	Sample tare mass after, g
A	1	0,4	0,1	8,855	6,301	2:31	22:33	13,050	17,259
	2	0,4	0,5	8,579	5,301	1:57	21:57	12,993	25,161
	3	0,4	1	10,748	7,257	1:55	21:59	21,119	39,399
	4	1,2	0,1	10,741	6,902	1:56	21:59	12,963	18,351
	5	1,2	0,5	10,754	7,471	1:57	21:59	12,973	25,002
	6	1,2	1	10,747	7,241	1:55	21:55	25,905	47,720
B	1	0,4	0,1	10,214	6,185	2:03	22:16	12,991	18,322
	2	0,4	0,5	10,507	6,742	2:44	22:48	13,049	25,941
	3	0,4	1	10,657	6,919	1:53	21:54	25,923	47,901
	4	1,2	0,1	10,670	6,739	2:07	22:10	12,880	18,076
	5	1,2	0,5	10,712	6,771	1:54	21:57	12,885	25,405
	6	1,2	1	10,493	6,077	1:48	21:48	49,247	71,536
	7	0,4	1	10,380	7,628	1:50	21:52	23,644	44,556
	8	1,2	0,1	7,627	4,496	1:57	22:01	12,982	17,676
C	1	0,4	0,1	10,571	6,501	-	-	12,900	18,231
	2	0,4	0,5	10,526	7,052	1:59	22:02	12,854	24,653
	3	0,4	1	10,533	6,544	2:02	22:05	25,948	47,290
	4	1,2	0,1	9,843	6,200	1:54	21:55	12,955	17,607
	5	1,2	0,5	9,613	5,996	2:00	22:03	12,974	24,458
	6	1,2	1	10,583	7,203	1:57	21:56	25,888	47,030
D	1	1,2	0,1	10,600	7,415	2:10	22:15	12,941	17,298
	2	1,2	0,3	7,411	3,935	2:08	22:08	12,961	21,713
	3	1,2	0,5	10,483	7,339	1:56	21:57	13,027	25,659
	4	1,2	0,7	7,338	3,892	1:52	21:53	25,995	43,118
	5	1,2	1	7,961	4,780	1:55	21:56	25,921	49,011

Appendix I, 2

Set	№	Needle, mm	Feedrate, ml/min	Seed mass before, g	Seed mass after, g	Feed start time, min:sec	Feed finish time, min:sec	Sample tare mass before, g	Sample tare mass after, g
E	1	1,2	0,1	10,536	7,293	2:07	22:07	12,965	17,556
	2	1,2	0,3	8,247	4,720	1:52	21:52	12,852	22,171
	3	1,2	0,5	10,359	6,883	1:51	21:51	13,004	25,316
	4	1,2	0,7	10,496	7,146	1:54	21:54	25,926	42,183
	5	1,2	1	9,030	4,654	1:47	21:49	25,878	49,427
F	1	1,2	0,1	10,712	6,854	2:05	22:08	12,966	18,195
	2	1,2	0,3	10,659	6,709	1:50	21:51	12,970	22,122
	3	1,2	0,5	10,617	7,504	1:52	21:52	12,953	24,771
	4	1,2	0,7	10,545	7,434	1:47	21:51	25,813	42,796
	5	1,2	1	8,007	4,453	1:48	21:47	26,027	49,181
G	1	1,2	0,1	10,475	8,606	4:36	24:42	13,011	16,578
	2	1,2	0,3	8,605	6,976	4:46	24:50	12,971	19,497
	3	1,2	0,5	6,971	5,408	2:58	23:06	12,958	22,234
	4	1,2	0,7	7,878	6,461	3:58	23:58	12,921	27,560
	5	1,2	1	6,456	5,046	2:57	23:19	25,845	47,537
H	1	1,2	0,1	10,456	9,073	3:15	23:58	12,936	15,465
	2	1,2	0,3	9,060	7,572	2:19	22:21	12,940	19,417
	3	1,2	0,5	7,568	6,296	2:14	22:16	12,902	23,764
	4	1,2	0,7	6,292	5,278	2:01	22:01	12,955	27,556
	5	1,2	1	5,275	3,855	2:06	22:07	25,767	46,824
I	1	1,2	0,1	10,116	8,519	3:02	23:18	12,919	16,184
	2	1,2	0,3	8,516	7,372	3:04	23:06	12,930	18,207
	3	1,2	0,5	7,367	5,727	2:07	22:08	12,890	24,345
	4	1,2	0,7	8,641	7,121	2:15	22:17	12,854	28,252
	5	1,2	1	7,116	5,342	2:31	22:30	25,697	46,728

Appendix I, 3

Set	№	Needle, mm	Feedrate, ml/min	Seed mass before, g	Seed mass after, g	Feed start time, min:sec	Feed finish time, min:sec	Sample tare mass before, g	Sample tare mass after, g
J	1	1,2	0,1	10,305	6,834	2:32	22:34	12,982	17,916
	2	1,2	0,3	8,375	4,860	2:13	22:13	12,938	21,982
	3	1,2	0,5	8,561	5,183	2:00	22:00	12,928	26,731
	4	1,2	0,7	9,085	5,792	1:54	21:54	12,842	29,848
	5	1,2	1	9,212	6,129	2:09	22:10	25,948	49,290
	6	1,2	0,7	9,165	6,459	2:01	22:00	12,961	29,980
K	1	1,2	1	0,000	0,000	0:00	20:00	23,558	38,760
	2	1,2	0,5	0,000	0,000	0:00	20:00	12,954	20,581
	3	1,2	0,1	0,000	0,000	0:00	20:15	10,061	11,384
	4	1,2	1	0,000	0,000	0:00	20:00	23,634	36,471
	5	1,2	0,5	0,000	0,000	0:00	20:03	12,970	20,614
	6	1,2	0,1	0,000	0,000	0:00	20:09	9,708	11,114
	7	0,4	1	0,000	0,000	0:00	20:06	25,934	40,314
	8	0,4	0,5	0,000	0,000	0:00	20:02	12,974	20,276
	9	1,2	0,3	0,000	0,000	0:00	20:00	12,922	17,349
	10	1,2	0,7	0,000	0,000	0:00	20:01	12,879	24,052

Set	№	Sample density, g/cm^3	Sample Cu concentration, ppm	Dilution factor	Feed density, g/cm^3	Feed Cu concentration, g/l	Continuous phase density, g/cm^3	Acorga M5460 concentration, mol/l
A	1	1,026	257,180	20	1,030	9,478	0,834	0,4
	2	1,026	373,950	20	1,030	9,478	0,834	0,4
	3	1,028	407,130	20	1,030	9,478	0,834	0,4
	4	1,030	323,130	20	1,030	9,478	0,834	0,4
	5	1,029	306,860	20	1,030	9,478	0,834	0,4
	6	1,029	413,060	20	1,030	9,478	0,834	0,4
B	1	1,027	370,660	20	1,030	8,422	0,835	0,4
	2	1,026	330,540	20	1,030	8,422	0,835	0,4
	3	1,028	385,850	20	1,030	8,422	0,835	0,4
	4	1,025	303,720	20	1,030	8,422	0,835	0,4
	5	1,029	324,050	20	1,030	8,422	0,835	0,4
	6	1,029	310,240	20	1,030	8,422	0,835	0,4
	7	1,028	420,490	20	1,031	9,518	0,835	0,4
	8	1,030	459,980	20	1,031	9,518	0,835	0,4
C	1	1,007	128,980	20	1,009	2,803	0,834	0,4
	2	1,007	127,810	20	1,009	2,803	0,834	0,4
	3	1,007	132,130	20	1,009	2,803	0,834	0,4
	4	1,007	116,980	20	1,009	2,803	0,834	0,4
	5	1,007	115,780	20	1,009	2,803	0,834	0,4
	6	1,007	123,230	20	1,009	2,803	0,834	0,4
D	1	1,028	403,390	20	1,030	9,627	0,835	0,4
	2	1,027	437,760	20	1,030	9,627	0,835	0,4
	3	1,028	424,650	20	1,030	9,627	0,835	0,4
	4	1,028	432,100	20	1,030	9,627	0,835	0,4
	5	1,028	422,310	20	1,030	9,627	0,835	0,4

Set	№	Sample density, g/cm^3	Sample Cu concentration, ppm	Dilution factor	Feed density, g/cm^3	Feed Cu concentration, g/l	Continuous phase density, g/cm^3	Acorga M5460 concentration, mol/l
E	1	1,027	434,050	20	1,030	10,289	0,832	0,4
	2	1,026	414,300	20	1,030	10,289	0,832	0,4
	3	1,028	446,980	20	1,030	10,289	0,832	0,4
	4	1,029	447,060	20	1,030	10,289	0,832	0,4
	5	1,028	433,190	20	1,030	10,289	0,832	0,4
F	1	1,026	385,870	20	1,030	9,058	0,832	0,4
	2	1,027	148,520	20	1,030	9,058	0,832	0,4
	3	1,028	222,760	20	1,030	9,058	0,832	0,4
	4	1,029	372,730	20	1,030	9,058	0,832	0,4
	5	1,029	215,840	20	1,030	9,058	0,832	0,4
G	1	1,022	404,560	20	1,031	10,336	0,834	0,4
	2	1,026	379,790	20	1,031	10,336	0,834	0,4
	3	1,018	404,070	20	1,031	10,336	0,834	0,4
	4	1,030	425,820	20	1,031	10,336	0,834	0,4
	5	1,030	442,910	20	1,031	10,336	0,821	0,4
H	1	1,029	389,750	20	1,031	10,336	0,821	0,2
	2	1,029	384,170	20	1,031	10,336	0,821	0,2
	3	1,029	411,970	20	1,031	10,336	0,821	0,2
	4	1,030	386,700	20	1,031	10,336	0,821	0,2
	5	1,030	424,870	20	1,031	10,336	0,821	0,2
I	1	1,028	466,480	20	1,031	10,336	0,813	0,1
	2	1,028	383,150	20	1,031	10,336	0,813	0,1
	3	1,030	453,150	20	1,031	10,336	0,813	0,1
	4	1,030	478,170	20	1,031	10,336	0,813	0,1
	5	1,030	502,770	20	1,031	10,336	0,813	0,1

Appendix II, 3

Set	№	Sample density, g/cm^3	Sample Cu concentration, ppm	Dilution factor	Feed density, g/cm^3	Feed Cu concentration, g/l	Continuous phase density, g/cm^3	Acorga M5460 concentration, mol/l
J	1	1,029	413,060	20	1,030	10,339	0,810	0,1
	2	1,028	361,460	20	1,030	10,339	0,810	0,1
	3	1,028	402,490	20	1,030	10,339	0,810	0,1
	4	1,029	394,940	20	1,030	10,339	0,810	0,1
	5	1,029	445,810	20	1,030	10,339	0,810	0,1
	6	1,027	463,130	20	1,030	10,339	0,832	0,4
K	1	0,834	138,130	2,5	0,830	10,438	1,031	0,4
	2	0,833	158,330	2,5	0,830	10,438	1,031	0,4
	3	0,834	113,580	2,5	0,830	10,438	1,031	0,4
	4	0,836	123,750	2,5	0,830	3,656	1,031	0,4
	5	0,834	162,280	2,5	0,830	3,656	1,031	0,4
	6	0,834	131,470	2,5	0,830	3,656	1,031	0,4
	7	0,833	160,270	2,5	0,830	10,438	1,031	0,4
	8	0,833	179,400	2,5	0,830	10,438	1,031	0,4
	9	0,836	160,040	2,5	0,833	9,600	1,031	0,4
	10	0,835	146,420	2,5	0,833	9,600	1,031	0,4

Set	№	d_{32}, m	Re_c	Pe_c	Sc_c	$Sh_{c,r}$	$Sh_{c,\infty}$	Sh_c	k_c, m/s	Sc_d	Sh_d	k_d, m/s
A	1	0,001	45,102	141075,853	3127,932	85,341	423,820	152,303	$3{,}025 \cdot 10^{-5}$	1213,828	52,815	$2{,}604 \cdot 10^{-5}$
	2	0,002	88,532	276921,318	3127,932	122,410	593,791	249,088	$3{,}718 \cdot 10^{-5}$	1213,828	101,865	$3{,}775 \cdot 10^{-5}$
	3	0,003	133,851	418676,869	3127,932	153,721	730,121	333,921	$3{,}809 \cdot 10^{-5}$	1213,828	157,850	$4{,}470 \cdot 10^{-5}$
	4	0,001	49,782	155715,189	3127,932	89,898	445,267	165,761	$3{,}532 \cdot 10^{-5}$	1213,828	57,746	$3{,}055 \cdot 10^{-5}$
	5	0,002	97,612	305324,828	3127,932	129,114	623,500	266,016	$3{,}625 \cdot 10^{-5}$	1213,828	112,800	$3{,}816 \cdot 10^{-5}$
	6	0,002	131,498	411315,995	3127,932	152,209	723,674	333,251	$4{,}188 \cdot 10^{-5}$	1213,828	154,868	$4{,}833 \cdot 10^{-5}$
B	1	0,001	25,539	79836,522	3126,058	63,543	318,828	102,035	$2{,}642 \cdot 10^{-5}$	1213,357	33,792	$2{,}172 \cdot 10^{-5}$
	2	0,002	67,949	212411,739	3126,058	106,073	520,049	205,426	$3{,}484 \cdot 10^{-5}$	1213,357	77,797	$3{,}276 \cdot 10^{-5}$
	3	0,002	111,797	349484,348	3126,058	139,083	667,066	296,646	$4{,}116 \cdot 10^{-5}$	1213,357	130,159	$4{,}484 \cdot 10^{-5}$
	4	0,001	42,822	133863,261	3126,058	83,033	412,844	150,156	$3{,}722 \cdot 10^{-5}$	1213,357	50,447	$3{,}104 \cdot 10^{-5}$
	5	0,002	97,985	306306,000	3126,058	129,358	624,501	267,623	$3{,}749 \cdot 10^{-5}$	1213,357	113,223	$3{,}938 \cdot 10^{-5}$
	6	0,002	124,367	388776,978	3126,058	147,533	703,567	319,406	$4{,}081 \cdot 10^{-5}$	1213,357	145,836	$4{,}626 \cdot 10^{-5}$
	7	0,002	113,944	356196,081	3126,058	140,552	673,441	300,194	$4{,}061 \cdot 10^{-5}$	1212,768	132,835	$4{,}462 \cdot 10^{-5}$
	8	0,002	62,145	194268,813	3126,058	101,121	497,344	193,879	$3{,}628 \cdot 10^{-5}$	1212,768	71,253	$3{,}311 \cdot 10^{-5}$
C	1	0,001	21,682	67861,729	3129,809	58,484	293,946	90,849	$2{,}431 \cdot 10^{-5}$	1239,219	30,422	$2{,}021 \cdot 10^{-5}$
	2	0,002	66,415	207865,599	3129,809	104,822	514,454	201,574	$3{,}367 \cdot 10^{-5}$	1239,219	75,810	$3{,}144 \cdot 10^{-5}$
	3	0,002	110,171	344813,762	3129,809	138,018	662,594	291,274	$3{,}804 \cdot 10^{-5}$	1239,219	127,641	$4{,}139 \cdot 10^{-5}$
	4	0,001	41,593	130177,184	3129,809	81,808	407,120	145,287	$3{,}271 \cdot 10^{-5}$	1239,219	49,070	$2{,}743 \cdot 10^{-5}$
	5	0,002	91,489	286342,012	3129,809	124,646	603,806	253,880	$3{,}574 \cdot 10^{-5}$	1239,219	104,990	$3{,}669 \cdot 10^{-5}$
	6	0,002	123,162	385474,124	3129,809	146,796	700,572	315,490	$3{,}856 \cdot 10^{-5}$	1239,219	143,733	$4{,}362 \cdot 10^{-5}$
D	1	0,002	68,091	212727,437	3124,186	106,171	520,435	204,935	$3{,}374 \cdot 10^{-5}$	1213,710	77,930	$3{,}186 \cdot 10^{-5}$
	2	0,002	98,142	306614,613	3124,186	129,446	624,815	267,130	$3{,}662 \cdot 10^{-5}$	1213,710	113,369	$3{,}858 \cdot 10^{-5}$
	3	0,002	109,056	340710,876	3124,186	137,166	658,640	288,098	$3{,}712 \cdot 10^{-5}$	1213,710	126,720	$4{,}053 \cdot 10^{-5}$
	4	0,002	125,816	393074,196	3124,186	148,456	707,444	320,560	$3{,}929 \cdot 10^{-5}$	1213,710	147,597	$4{,}491 \cdot 10^{-5}$
	5	0,002	143,736	449056,585	3124,186	159,903	756,146	354,659	$4{,}207 \cdot 10^{-5}$	1213,710	170,326	$5{,}016 \cdot 10^{-5}$

Set	№	d_{32}, m	Re_c	Pe_c	Sc_c	$Sh_{c,r}$	$Sh_{c,\infty}$	Sh_c	k_c, m/s	Sc_d	Sh_d	k_d, m/s
E	1	0,002	65,376	204909,737	3134,321	103,989	510,783	198,541	$3{,}215 \cdot 10^{-5}$	1213,121	74,983	$3{,}014 \cdot 10^{-5}$
	2	0,002	93,894	294294,775	3134,321	126,484	612,134	258,154	$3{,}497 \cdot 10^{-5}$	1213,121	108,438	$3{,}647 \cdot 10^{-5}$
	3	0,002	100,914	316296,666	3134,321	131,577	634,603	273,710	$3{,}756 \cdot 10^{-5}$	1213,121	116,966	$3{,}984 \cdot 10^{-5}$
	4	0,002	121,493	380797,504	3134,321	145,757	696,309	315,074	$4{,}123 \cdot 10^{-5}$	1213,121	142,458	$4{,}629 \cdot 10^{-5}$
	5	0,002	149,870	469741,717	3134,321	163,869	773,365	366,851	$4{,}301 \cdot 10^{-5}$	1213,121	178,558	$5{,}198 \cdot 10^{-5}$
F	1	0,002	68,456	214639,333	3135,452	106,601	522,769	206,073	$3{,}363 \cdot 10^{-5}$	1213,239	78,498	$3{,}180 \cdot 10^{-5}$
	2	0,002	90,662	284265,222	3135,452	124,103	601,613	251,900	$3{,}492 \cdot 10^{-5}$	1213,239	104,564	$3{,}598 \cdot 10^{-5}$
	3	0,002	110,405	346170,479	3135,452	138,261	663,896	292,467	$3{,}855 \cdot 10^{-5}$	1213,239	128,663	$4{,}211 \cdot 10^{-5}$
	4	0,002	132,498	415439,680	3135,452	152,973	727,292	333,707	$3{,}987 \cdot 10^{-5}$	1213,239	156,373	$4{,}638 \cdot 10^{-5}$
	5	0,002	159,868	501258,456	3135,452	169,953	798,888	387,116	$4{,}637 \cdot 10^{-5}$	1213,239	191,521	$5{,}696 \cdot 10^{-5}$
G	1	0,003	152,531	476877,155	3126,433	165,360	779,217	364,883	$3{,}710 \cdot 10^{-5}$	1212,533	181,734	$4{,}588 \cdot 10^{-5}$
	2	0,003	161,949	506322,936	3126,433	171,035	802,914	382,524	$3{,}888 \cdot 10^{-5}$	1212,533	193,912	$4{,}893 \cdot 10^{-5}$
	3	0,003	239,978	750276,617	3126,433	214,125	977,385	509,071	$4{,}278 \cdot 10^{-5}$	1212,533	297,304	$6{,}202 \cdot 10^{-5}$
	4	0,004	286,680	896286,128	3126,433	237,481	1068,264	579,656	$4{,}530 \cdot 10^{-5}$	1212,533	360,687	$6{,}999 \cdot 10^{-5}$
	5	0,004	301,999	944179,830	3126,433	244,848	1096,434	601,829	$4{,}592 \cdot 10^{-5}$	1212,533	381,654	$7{,}230 \cdot 10^{-5}$
H	1	0,003	231,879	737145,764	3179,010	211,073	968,795	508,739	$4{,}834 \cdot 10^{-5}$	1212,533	289,411	$6{,}828 \cdot 10^{-5}$
	2	0,003	195,414	621221,515	3179,010	191,323	889,361	448,527	$4{,}552 \cdot 10^{-5}$	1212,533	240,236	$6{,}053 \cdot 10^{-5}$
	3	0,003	235,339	748144,926	3179,010	212,887	975,996	512,085	$4{,}665 \cdot 10^{-5}$	1212,533	294,114	$6{,}652 \cdot 10^{-5}$
	4	0,004	307,772	978410,481	3179,010	248,958	1116,132	621,583	$5{,}006 \cdot 10^{-5}$	1212,533	393,732	$7{,}873 \cdot 10^{-5}$
	5	0,004	336,999	1071322,522	3179,010	262,661	1167,926	664,513	$5{,}214 \cdot 10^{-5}$	1212,533	434,433	$8{,}463 \cdot 10^{-5}$
I	1	0,003	278,120	892961,526	3210,702	235,362	1066,280	580,777	$4{,}824 \cdot 10^{-5}$	1212,533	354,934	$7{,}319 \cdot 10^{-5}$
	2	0,003	236,657	759835,158	3210,702	214,275	983,591	522,107	$5{,}096 \cdot 10^{-5}$	1212,533	297,754	$7{,}216 \cdot 10^{-5}$
	3	0,004	299,960	963082,000	3210,702	246,025	1107,355	614,671	$5{,}030 \cdot 10^{-5}$	1212,533	385,319	$7{,}828 \cdot 10^{-5}$
	4	0,004	314,696	1010393,920	3210,702	253,070	1134,228	636,611	$5{,}124 \cdot 10^{-5}$	1212,533	405,910	$8{,}112 \cdot 10^{-5}$
	5	0,004	324,672	1042426,742	3210,702	257,776	1152,067	652,199	$5{,}259 \cdot 10^{-5}$	1212,533	419,889	$8{,}406 \cdot 10^{-5}$

Set	№	d_{32}, m	Re_c	Pe_c	Sc_c	$Sh_{c,r}$	$Sh_{c,\infty}$	Sh_c	k_c, m/s	Sc_d	Sh_d	k_d, m/s
J	1	0,003	152,181	490056,237	3220,214	166,758	789,911	376,168	$4{,}208 \cdot 10^{-5}$	1213,710	184,495	$5{,}124 \cdot 10^{-5}$
	2	0,003	203,055	653880,231	3220,214	196,396	912,440	466,372	$4{,}733 \cdot 10^{-5}$	1213,710	252,420	$6{,}359 \cdot 10^{-5}$
	3	0,003	235,155	757250,097	3220,214	213,696	981,917	519,024	$4{,}938 \cdot 10^{-5}$	1213,710	296,170	$6{,}996 \cdot 10^{-5}$
	4	0,004	327,584	1054889,444	3220,214	259,393	1158,934	657,140	$5{,}236 \cdot 10^{-5}$	1213,710	424,661	$8{,}401 \cdot 10^{-5}$
	5	0,003	250,175	805615,571	3220,214	221,498	1012,789	546,399	$5{,}345 \cdot 10^{-5}$	1213,710	316,821	$7{,}694 \cdot 10^{-5}$
	6	0,003	168,780	529392,615	3136,582	175,261	821,002	396,977	$4{,}111 \cdot 10^{-5}$	1213,710	203,147	$5{,}222 \cdot 10^{-5}$
K	1	0,004	556,572	675451,998	1213,592	258,602	927,368	466,868	$8{,}294 \cdot 10^{-5}$	3143,007	649,130	$4{,}645 \cdot 10^{-5}$
	2	0,004	512,375	621814,769	1213,592	245,842	889,786	441,082	$8{,}370 \cdot 10^{-5}$	3143,007	595,085	$4{,}548 \cdot 10^{-5}$
	3	0,003	449,943	546047,910	1213,592	227,213	833,816	402,746	$8{,}334 \cdot 10^{-5}$	3143,007	519,036	$4{,}326 \cdot 10^{-5}$
	4	0,004	572,870	695230,664	1213,592	263,227	940,848	478,309	$8{,}669 \cdot 10^{-5}$	3143,007	669,096	$4{,}884 \cdot 10^{-5}$
	5	0,004	540,047	655397,168	1213,592	253,869	913,497	456,003	$8{,}071 \cdot 10^{-5}$	3143,007	628,904	$4{,}483 \cdot 10^{-5}$
	6	0,004	503,712	611300,638	1213,592	243,302	882,231	434,560	$8{,}104 \cdot 10^{-5}$	3143,007	584,510	$4{,}390 \cdot 10^{-5}$
	7	0,003	376,113	456447,710	1213,592	204,071	762,343	356,533	$8{,}592 \cdot 10^{-5}$	3143,007	429,657	$4{,}171 \cdot 10^{-5}$
	8	0,003	312,454	379192,343	1213,592	182,881	694,840	314,091	$8{,}780 \cdot 10^{-5}$	3143,007	353,235	$3{,}977 \cdot 10^{-5}$
	9	0,004	454,441	551505,473	1213,592	228,581	837,973	404,673	$8{,}145 \cdot 10^{-5}$	3130,184	525,130	$4{,}257 \cdot 10^{-5}$
	10	0,004	518,509	629258,905	1213,592	247,633	895,096	444,202	$8{,}259 \cdot 10^{-5}$	3130,184	603,308	$4{,}518 \cdot 10^{-5}$